Effects of Calibration Spectra on Mammographic Exposure Measurement

by

JOHN GERARD COLETTI

A dissertation submitted in partial fulfillment

of the requirements for the degree of

Doctor of Philosophy

(Medical Physics)

at the

UNIVERSITY OF WISCONSIN - MADISON

1995

Effects of Calibration Spectra on Mammographic Exposure Measurement

by

John G. Coletti

Under the supervision of Professor Paul M. DeLuca

At the University of Wisconsin - Madison

There are currently no National Institute of Standards and Technology (NIST) standard molybdenum anode x-ray beams to calibrate ionization chambers employed to measure exposure from mammographic imaging systems. The current beams employed for the calibration of such ionization chambers are tungsten anode / aluminum filtered orthovoltage beams. These tungsten beams are matched with respect to accelerating potential (kVp) and half-value layer (HVL) to the imaging beams. Historically this tungsten / aluminum combination was established for low-voltage x-ray therapy applications. The effects on the accuracy of the measurement of mammographic exposure due to the differences in the energy spectra of the calibration and clinical imaging beams have been investigated. The clinical and calibration x-ray beams have been characterized to enable the calibration of ionization chambers for accurate mammographic exposure measurements. The beams were characterized with regard to kVp, first and second half-value layers and photon-energy spectra, measured with a high-purity germanium spectrometer system. A variable-

length free-air ionization chamber was designed and developed for the mammography energy region to enable absolute exposure measurements in the x-ray beams. This free-air chamber was compared directly against the Ritz 20-100 kV free-air chamber at the NIST on their low-energy tungsten x-ray range. Disagreement between the Ritz and Attix free-air chambers is less than 0.24%, well within the uncertainty expected for such an intercomparison. A variety of typical ionization chambers were calibrated against the free-air chamber and the response of these chambers versus the beam parameters are presented. Results of this research show that all current mammographic ionization chambers measure exposure accurately to within 5% on clinical mammography units if the chambers have been calibrated using the current tungsten anode, aluminum filtered calibration beams at the appropriate HVL and kVp. Measurements of HVL for the tungsten and molybdenum beams were performed with four of the ionization chambers to show the effect of chamber energy response on the accuracy of HVL measurement. Better accuracy in exposure measurements will result from calibrations performed on molybdenum anode calibration beams being established as a continuation of this research.

Acknowledgements

I am very fortunate to have benefited from the guidance and support of many faculty and staff while pursuing my graduate degree at the UW-Madison. First I would like to thank P.M. DeLuca, my thesis advisor, for his contributions and encouragement throughout my tenure in the Medical Physics Department. Sincere thanks are extended to L.A. DeWerd for proposing this project to me and providing the facilities, support and daily guidance needed to bring it to completion. D.W. Pearson deserves great praise for sharing his time, invaluable experimental insight and technical skills. I also thank F.H. Attix for sitting me down to detailed discussions on free-air ionization chambers and metrology and for proposing the design of free-air chamber constructed for this study. T.R. Mackie is thanked for his excellent course in dosimetry and the many discussions that followed. M.P. Seidband is thanked for discussions on diagnostic x-ray spectroscopy, but not for his jokes. M.A. Ross is thanked for sharing his expertice in monte carlo transport, his CPU and his friendship.

Special thanks are extended to the calibration laboratory where I served my time, including F. Grenzow, D. Anderson, C. Gifford, N.B. Chiu, C. Reynolds and J. Schwantz. Special thanks to J.A. Micka for sharing his friendship, his knowledge in metrology and his shit. Thanks to machine shop G.R. Frank - damn you're good.

Thanks to all the students who make medical physics at UW what it is, especially B. Murphy for helping me keep things in perspective, J.G. Miranda for doing all the reading that I should have done, E. Hendee for continuing the tradition, J. Polzin for sharing living expenses and to my friend, my friend, M. Zaini. Thanks also to those who welcomed me to Madison and have since moved on, including D. Kruger, R.A. Pooley, S.J. Swerdloff, C. Endres and T. Oakes.

Thanks to K. McSherry for always being there ready to help, to C. Schutz for always smiling and keeping things organized and to B. Ziemer and K. Hurd for all you do.

Thanks are extended to B. Coursey, S. Seltzer, P.J. Lamperti and M. Johnson from the National Institute of Standards and Technology and H.T. Heaton, F. Cerra and M. Walker of the Center for Devices and Radiologic Health of the U.S. Food and Drug Administration for their collaboration on this project.

Finally, I thank my wife Jean for her love and support and my family for their encouragement in all that I pursue.

TABLE OF CONTENTS

List of Figures

List of Tables

CHAPTER 1 INTRODUCTION

1.1 Exposure Measurement in Mammography

Mammography is a technically exacting radiological examination of the breast. Breast cancer is the most prevalent nonskin cancer among women with over 175,000 new cases each year. The 45,000 breast cancer-related deaths annually make it the second most deadly. Regular screening mammography can often identify possible disease at an early stage; diagnostic mammography is valuable in confirming the presence of breast cancer [1]. High quality mammographic procedures are vital to ensure that cancerous breast lesions are detected and treated early.

Mammography employs a molybdenum rotating anode x-ray tube and single-phase high-frequency generator operating between 23 and 35 kVp. The size of the electron beam incident on the anode, referred to as the focal spot size, is 0.3 to 0.4 mm for regular screening while a 0.1 mm spot size is used for magnification. A molybdenum anode, which produces a continuous bremsstrahlung spectrum plus two sharp K-characteristic lines at approximately 17.5 and 19.6 keV, is employed. These characteristic photon energies are ideal for providing high-contrast images of average thickness breasts at an acceptable patient absorbed dose. An additional 30 μm of molybdenum is added to reduce the number of low energy photons incident the patient which increase absorbed dose but do not contribute significantly to the image. With a K-edge at 20.0 keV, the molybdenum filter also reduces the number of photons above 20 keV which produce noticeably lower image contrast. Rhodium anode systems with rhodium filtration have recently been introduced for imaging thicker or more dense breasts. Rhodium's characteristic x-rays at 20.2 and 22.7 keV and K-edge at 23.2 keV yield an x-ray beam with higher effective energy than a molybdenum

anode beam, resulting in more primary photons reaching the film cassette and forming a radiographic image.

A radiographic image is produced by differential attenuation of the primary beam by the patient's anatomy. Scattered radiation from the patient reaching the film tends to mask the contrast produced by the primary thereby reducing the quality of the image. This scattered radiation may be removed by a grid placed between the film and the patient. A grid consists of an array of lead strips separated by spacers of low density material. Modern grids may have 40 lines per centimeter. A moving grid is used in mammography to remove of the image of the lead strips on the radiograph. The grid improves contrast significantly; but the dose is increased by a factor of two to three. To reduce the radiation exposure, high-resolution intensifying screens are employed. The screens are constructed of a plastic base upon which is mounted a partially reflecting coating followed by a layer of fluorescent material such as calcium tungstate or gadolinium oxysulphide. The cassette maintains continuous contact between the film and screen to avoid loss of resolution through spreading of the emitted light. In more recent years, dual screens and double emulsion film have been introduced to further reduce patient exposure, but they haven't found high acceptance, primarily due to reduced resolution.

To maintain the optimal performance of a mammography system, a program of quality assurance (QA) is essential [2]. A QA program will identify imaging performance problems as well as monitor patient exposure. A wide variety of QA tests are performed on a mammography system including: image quality evaluation with a resolution and contrast phantom, measurement of surface exposure with an ionization chamber and calculation of mean glandular dose, measurement of half-value layer (HVL) and electron beam spot size, light field accuracy and alignment of x-ray field to film cassette, accuracy and reproducibility of electron accelerating potential (kVp), linearity of electron beam current and exposure time,

exposure output and reproducibility, performance of electronic exposure control devices and analysis of imaging problems and retakes. The ACR Manual: Medical Physicist's Section summarizes these tests[2]. The results of two of the test procedures, measurement of surface exposure and measurement of half-value layer, depend heavily on the calibration and energy response of the ionization chamber used for such measurements.

The adequacy of filtration in a mammography system is checked by measuring the HVL in mm of aluminum. If too little filtration is present, low energy photons below 10 keV will expose the patient, increase her dose, but contribute few photons to the image receptor. Too much filtration reduces the usable x-ray output and can result in excessively long exposure times. This longer exposure time could lead to blurring due to increased patient motion. The kVp may be raised to increase the number of photons, but these higher energy photons produce lower contrast images.

The HVL is defined as the thickness of some standard material required to reduce the exposure of an x-ray beam to half its original value. In practice, an in-air exposure measurement is made , and then thin sheets of aluminum are added until the exposure is reduced to one half. The addition of aluminum to the beam, effectively hardens the beam spectrum. Wagner et al. have shown that severe energy dependence of the ionization chamber in this energy range will result in significant errors, greater than 10%, in HVL determination. The change in calibration factor over the range of mammography beam qualities should be less than 5% in order to adequately measure HVL [3].

The absorbed dose to the glandular tissue is calculated since glandular tissue was determined to be the most radiosensitive tissue in the breast. This dose is referred to as mean glandular dose and best represents the radiation risk to the patient [4]. First the exposure is determined either from ionization chamber or thermoluminescent dosimeter measurements. This exposure is then converted to absorbed dose by a conversion factor [5] which depends

on breast composition and thickness and imaging beam half-value layer. An inaccurate calibration of the ionization chamber and an inaccurate measure of HVL would combine and result in inaccurate absorbed dose determination. Patient dose is also affected by components of the imaging system as well as film speed, processing technique and film density.

There are no known short-term health effects from diagnostic exposures of x-ray radiation and the risk of potential long-term effects has a larger uncertainty. Therefore diagnostic exposure measurements need not be performed with either the accuracy or precision needed for therapeutic dose measurements. However, radiation exposure is a major concern among the patient population. The radiation risk from mammographic screening is stated in BEIR V to have a 10 year minimum latency period, with no excess breast cancer risk observed within ten years of exposure [6]. The incidence of breast cancer increases with age at a much faster rate than the excess relative risk from mammographic screening; the excess relative cancer risk from 0.1 Gy acute absorbed dose is estimated at 0.05 per 1000 person years. However small, any reduction in radiation dose during screening is certainly desirable. If the greater accuracy in dose measurement results in lower doses, equal benefit would be achieved at lower risk. It may also be advantageous to extend mammography to selected younger populations, potentially finding earlier staged cancers and increasing life expectancy. According to Wagner et al. [7] "With advances in our knowledge about risks from exposures to low levels of ionizing radiation, the need to accurately assess absorbed doses from diagnostic x-ray examinations has increased." Accurate knowledge of absorbed dose and risk is important for mammography since screening of the population is performed involving large numbers of women, women without clinical signs of breast cancer, being exposed to ionizing radiation. The ACR has set an upper limit of 3 mGy per image for each breast. NEXT data from 1992 [8] have an average mean glandular dose of

1.8 mGy, over ten times the average dose for a chest radiograph of 0.12 mGy. More recent TLD data analyzed by Gentry and DeWerd [9] show an average mean glandular absorbed dose of 1.5 mGy per breast.

To convert the measurement of charge collected from the ionization chamber to exposure requires multiplication by a calibration factor assigned to that chamber. Since the chamber's response varies with the energy of the photon beam in which the measurements are made, calibration factors are assigned to chambers using calibration beams that are matched to the clinical beam parameters of kVp and HVL. The National Institute of Standards and Technology (NIST) maintains the national exposure standards for diagnostic energies on a constant potential tungsten anode aluminum filtered x-ray system and associated free-air ionization chamber [10]. A transfer standard is calibrated against the free-air chamber for secondary calibration facilities such as the UW-Madison Accredited Dosimetry Calibration Laboratory (ADCL). NIST assigns an uncertainty of ±1% to its calibrations. Customer chambers are then calibrated against this transfer standard, again on tungsten anode aluminum filtered constant potential beams. The UW-ADCL assigns an uncertainty of ±2% to its diagnostic calibrations.

The Mammography Quality Standards Act of 1992 [11] set new standards for mammography facility accreditation. Regulatory agencies in some states adopted limits on allowable exposures from diagnostic studies. Manufacturers are attempting to develop imaging systems which minimize radiation exposure while maximizing radiographic image quality. Quality assurance on mammography systems requires that the physicist monitor exposures and image quality to assure that radiation levels and radiographic quality are within acceptable norms. All these regulations require the accurate measurement of output exposure from mammographic imaging systems, yet little has been done in investigating the accuracy in exposure measurements achievable with the current calibration protocol using

tungsten anode aluminum filtered calibration beams. A recent study by Law [12] compares calibration factors assigned to ionization chambers on both tungsten and molybdenum anode beams. The results show at least a 2% variation in calibration factors when comparing tungsten and molybdenum beams. No absolute dosimeter was used in that study. The present research investigates the accuracy of the current exposure calibration of ionization chambers used in mammography and the establishment of exposure standards in the mammography energy region.

1.2 Research Goals

This work attempts to evaluate the effect of mammographic x-ray tube anode and filter composition on the response of ionization chambers used to measure the exposure output and half-value layer from clinical mammography systems. The establishment of reference exposure standards for diagnostic chamber calibrations in the mammography energy region is also proposed. To accomplish this goal, the following have been completed:

i) Design, construct and characterize free-air ionization chamber.

A variable-length free-air ionization chamber was designed and constructed to enable absolute exposure measurements [13] in x-ray beams up to 50 kVp. This Attix-style chamber [14] was directly compared with NIST's Ritz low-energy free-air ionization chamber on NIST's tungsten anode aluminum filtered beams to ensure its accuracy as an exposure standard in the mammography energy range [15].

ii) Characterize calibration and clinical x-ray beams.

The kVp, half-value layer in aluminum, homogeneity coefficient and photon energy spectrum were measured for each of the beams in this investigation. These data help

to characterize the differences between the clinical and calibration x-ray beams which effect the response of the ionization chambers.

iii) Compare response of ionization chambers on all x-ray beams.

All current models of mammography ionization chambers, as well as a few chambers designed for general diagnostic energies, were calibrated against the UW-FAC on tungsten anode \ aluminum filtered and molybdenum anode \ molybdenum filtered x-ray beams. Calibration factors versus beam parameters are reported for each of these chambers.

1.3 Organization of Thesis

In this first chapter I provide an overview the current state of ionization chamber applications and calibrations in the mammography energy region as well as define the goals of this research project. In Chapter 2, the tungsten and molybdenum anode x-ray sources used in the calibration procedures are described along with their beam characteristics. Chapter 3 describes the spectrometer system used to make the spectral measurements of the calibration beams, the calibration of the spectrometer system and the photon energy spectra for the calibration beams. Chapter 4 begins with the description of two different designs of free-air ionization chambers, followed by a detailed description of the UW free-air chamber and concludes with the results of an intercomparison of the two FACs on tungsten anode beams at mammography energies. In Chapter 5 the response of a representative collection of diagnostic ionization chambers versus beam parameter of half-value layer is presented. Chapter 6 concisely presents the results of the project and gives direction to areas that may yet need further investigation. The thesis concludes with an appendix describing the monte carlo calculations that were performed to arrive at scatter photon correction factors for the free-air chamber on all the calibration beams.

1.4 References

[1] "The National Strategic Plan for the Early Detection and Control of Breast and Cervical Cancers," U.S. Department of Health and Human Services, 1993.

[2] American College of Radiology, Committee on Quality Assurance in Mammography. Medical Physicist's Manual. American Cancer Society (1992).

[3] L.K. Wagner, B.R. Archer, and F. Cerra, "On the Measurements of Half-Value Layer in Film-Screen Mammography", Med. Phys. **17**:989-997 (1990).

[4] AAPM Report No. 29. Equipment requirements and quality control for mammography. Report of Task Group No.7: Diagnostic x-ray imaging, Martin J. Yaffe, chairman. New York: *Am Assoc. Physicists Med*; August 1990.

[5] X. Wu, G.T. Barnes, and D.M. Tucker, "Spectral dependence of glandular tissue dose in screen-film mammography," Radiology **179**: 143-148 (1991).

[6] National Research Council, Committee on the Biological Effects of Ionizing Radiation. Health Effects of Exposure to Low Levels of Ionizing Radiation (BEIR V). Washington, D.C.: National Academy Press (1991).

[7] L.K. Wagner, D.P. Fontenla, C. Kimme-Smith, L.N. Rothenberg, J. Shepard and J.M. Boone, "Recommendations on performance characteristics of diagnostic exposure meters: Report of AAPM Diagnostic X-Ray Imaging Task Group No.6" Med. Phys. **19**:231 (1992).

[8] B.J. Conway, O.H. Suleiman, F.G. Rueter, R.G. Antonsen and R.J. Slayton, "National Survey of Mammographic Facilities in 1985, 1988 and 1992," Radiology 1994; 191: 323-330.

[9] J.R. Gentry and L.A. DeWerd, " TLD Measurements of *In-Vivo* Mammographic Exposures and the Calculated mean glandular dose across the United States," submitted to Med. Phys. (1995).

[10] P.J. Lamperti, T.P. Loftus, and R. Loevinger, "Calibration of X-Ray and Gamma-Ray Measuring Instruments," NBS Special Publication 250-16 (1988).

[11] Mammography Quality Standards Act of 1992, Public Law 102-539.

[12] J. Law, "Calibration of ion chambers for use in mammography," Br. J. Radiol. 66: 51-54 (1993).

[13] J.G. Coletti, D.W. Pearson, and L.A. DeWerd "Mammography exposure standard: Design and characterization of a free-air ionization chamber," Rev. Sci. Instrum. 66(3), March 1995.

[14] F.H. Attix, "Electronic Equilibrium in Free-Air Chambers and a Proposed New Chamber Design," Naval Res. Lab. Rep. No. 5646 (1961).

[15] J.G. Coletti, D.W. Pearson, L.A. DeWerd, C.M. Johnson and P.J. Lamperti "Comparison of Exposure Standards in the Mammography X-ray Region," in preparation.

CHAPTER 2 X-RAY SOURCES

Clinical and calibration x-ray systems are designed for different applications and therefore contain inherent differences. The effect of these differences on the measurement of exposure is the subject of this thesis. This section describes the differences in the x-ray systems, while the differences in the x-ray beam characteristics are addressed later.

2.1.1 NIST Low-Energy X-Ray Source

The NIST low-energy x-ray range uses a tungsten anode tube to generate x-rays at applied potentials of 10 kV to 100 kV with a constant-potential generator. The tube and a safety shutter are enclosed in a lead and steel housing. Outside the housing are the timing shutter, the beam collimator, aluminum filter packs, and a monitor chamber. Inherent tube filtration is a nominal 1 mm of beryllium. Chambers are positioned in the horizontal beam at distances up to 2 m from the tube focus using a cart on parallel tracks. The position of the chamber relative the free-air chamber is determined using a telescope and vernier.

NIST x-ray beam qualities offered for exposure calibration of measuring instruments are divided into groups according to beam filtration, i.e., light, moderate and heavy filtration [1]. The qualities for each group were chosen so that the x-ray tube constant potentials plotted versus half-value layer of the beam fall on a smooth curve. The beam codes consist of the letter L, M or H, followed by the generating constant potential in kilovolts. For example, M30 indicates a moderate filtration and 30 kV constant potential. Table 2.1 gives a listing of the beam codes relevant to this study.

Selection of beam qualities for instrument calibration depends on the situation of interest. The M qualities are usually used for calibration for radiation therapy and diagnostic radiology. The L series beams are for calibration of instruments for measurement of

Table 2.1 First and second half value layers and homogeneity coefficients for NIST and UW-ADCL tungsten anode calibration beams. NIST data taken from NBS Special Publication 250-16 (1988).

	NIST @ 50 cm			UW-ADCL @ 100 cm		
Beam code	**HVL-1 (mm Al)**	**HVL-2 (mm Al)**	**H.C. %**	**HVL-1 (mm Al)**	**HVL-2 (mm Al)**	**H.C. %**
M20	0.152	0.192	79.2	0.147	0.198	74.2
M30	0.36	0.563	63.9	0.369	0.565	65.3
M40	0.73	1.106	66.0	0.773	1.119	69.1
M50	1.02	1.546	66.0	1.062	1.606	66.1
L30	0.22	0.37	59.5	0.264	0.442	59.7
L40	0.49	0.86	57.0	0.524	0.862	60.8
L50	0.75	1.29	58.1	0.781	1.286	60.7

unfiltered or lightly filtered beams that give high exposure rates, as is often the case in radiation biology and superficial therapy. The H qualities are usually used for calibration for radiation protection, since these beams have the narrowest spectrum at each generating potential, most nearly approximating the radiation penetrating a protective barrier.

2.1.2 UW-Madison ADCL X-Ray Sources

The UW-ADCL Philips MG 163 - 323 x-ray system is a three phase high frequency stationary anode x-ray system with tungsten anode and aluminum filtration with kVp range from 0 to 320 kVp. Nominal electron beam spot size is 4.0 mm (optional 2.0 mm spot). Tube current (0-20 mA) and exposure time are independent. The tube head is oil cooled. The x-ray tube is mounted along a wall yielding a horizontal beam; a cart on parallel tracks enables chamber positioning at various distances from the source. Chamber position is determined by a cross laser marking the 100 cm point and a line laser marking the tube anode/cathode axis. Exposure time is controlled through a timer / shutter system. The beam is collimated with a primary lead collimator immediately outside of the tube and a secondary square collimator 30 cm from the tube to form a 10 cm square field at 100 cm. Inherent filtration is 2.0 mm of beryllium. Additional aluminum filtration is added to the beams to match NIST moderately filtered x-ray beam half-value layers and homogeneity coefficients. A thin window transmission ionization chamber is employed to monitor tube output.

The clinical mammography x-ray system employed in this research is the Ausonics model Alpha HF manufactured by Ausonics Corporation of Milwaukee in 1988. The clinical x-ray unit is single-phase, high frequency (2.5 kHz), cathode-grounding type with a rotating molybdenum anode x-ray tube, 1.0 mm beryllium window and 0.03 mm molybdenum filter. The range of kV is 23-34 kVp with the molybdenum filter or 35 to 49 kVp with the optional 0.5 mm aluminum filter. System logic was adjusted to enable the 0.03 mm molybdenum filter to remain in the beam at all kVps. Desired mAs is achieved with a constant tube current

at each kVp setting (approximately 100 mA) and varied exposure times. Nominal electron beam spot size is 0.4 mm (optional 0.1 mm spot for magnification work) and the target angle is 16°. Source to image distance is 0.6 m. Various cones can be attached to vary the field size. A thin window parallel plate transmission ionization chamber is employed just outside the cone to monitor variations in the tube output. The monitor chamber plates are tin evaporated onto 60 μm thick mylar. The head assembly was removed from the generator and mounted on a wall to yield a vertical beam. The image receptor support and cassette holder were removed.

2.2 Focal Spot Size

To enable the imaging of microcalcifications in breasts, the size of the electron beam incident on the anode (focal spot) in most mammography systems is nominally 0.3 to 0.5 mm. This focal spot size is dictated by the imaging geometry of the system. The use of larger focal spots significantly degrades the image quality. The use of too small a focal spot will limit the maximum mAs of the system, therefore requiring longer exposure times, increasing the chance of patient motion, or the use of higher kVp, which reduces the image contrast.

The focal spot size on calibration beams are on the order of 4 to 5 mm, quite larger than those on imaging systems. This is possible because the goal of these systems is to provide a uniform field of high intensity x-rays, not imaging.

The focal spot size of each of the tubes in this study were measured using a standard pinhole device provided by Standard Imaging (Middleton, WI). The tool consisted of an array of 0.1 mm pinholes in a lead sheet. The focal spot size was determined by positioning the pinhole array in the x-ray beam and exposing a film some distance behind the array. The focal spot size, ℓ_{spot}, was then determined from

$$\ell_{spot} = \frac{\ell_{film}}{\frac{d_{film}}{d_{array}} - 1}$$

where ℓ_{film} is the size of the images on the film,

d_{array} is the distance between the pinholes on the array and

d_{film} the distance between the images on the film.

The focal spot size on the UW orthovoltage machine were determined to be 4.1 mm x 4.6 mm for the large focal spot used during calibrations. A small focal spot option measured 1.7 mm x 2.0 mm. The molybdenum anode clinical tube has a focal spot size of 1.8 mm x 1.2 mm .

2.3 Field Flatness

Since the size of most mammography ionization chambers are large, 10 to 50 mm in diameter, the uniformity or flatness of the x-ray fields covering the chambers is an important parameter. Calibration beams are set-up to provide a uniform field of at least 10 cm square at a distance of 100 cm. Clinical mammography beams take advantage of the heel effect in imaging breasts, positioning the chest wall closest to the tube anode.

The x-ray field flatness of the UW-ADCL orthovoltage and clinical mammography beams were determined at 50 and 100 cm. A sheet of Kodak redipack XTL film was positioned perpendicular to each beam axis at 50 and 100 cm. The orthovoltage film was exposed with UW-ADCL 20-M beam to 25 and 100 mAs; the mammography film was exposed to a 28 kVp beam to 25 and 100 mAs. (Please refer to Tables 2.1 and 2.2 for explanation of tungsten and molybdenum beam code descriptors.) The films were developed and then scanned with a flatbed scanner. Normalized density data are plotted versus position for two data sets orthogonally bisecting the field and are shown in Fig. 2.1 and Fig. 2.2.

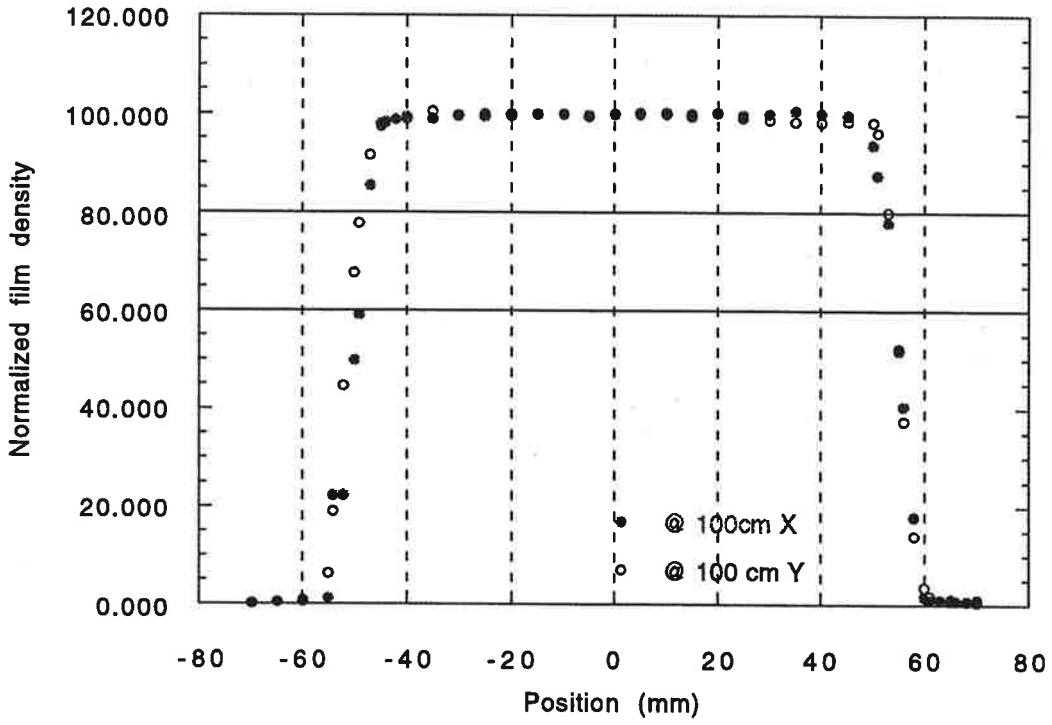

Figure 2.1 Plot of normalized film density versus distance from beam center for UW-ADCL tungsten calibration beam at 1 m.

Figure 2.2 Plot of normalized film density versus distance from beam center for UW-ADCL molybdenum anode clinical mammography beam a) along anode/cathode axis and b) perpendicular to anode/cathode axis.

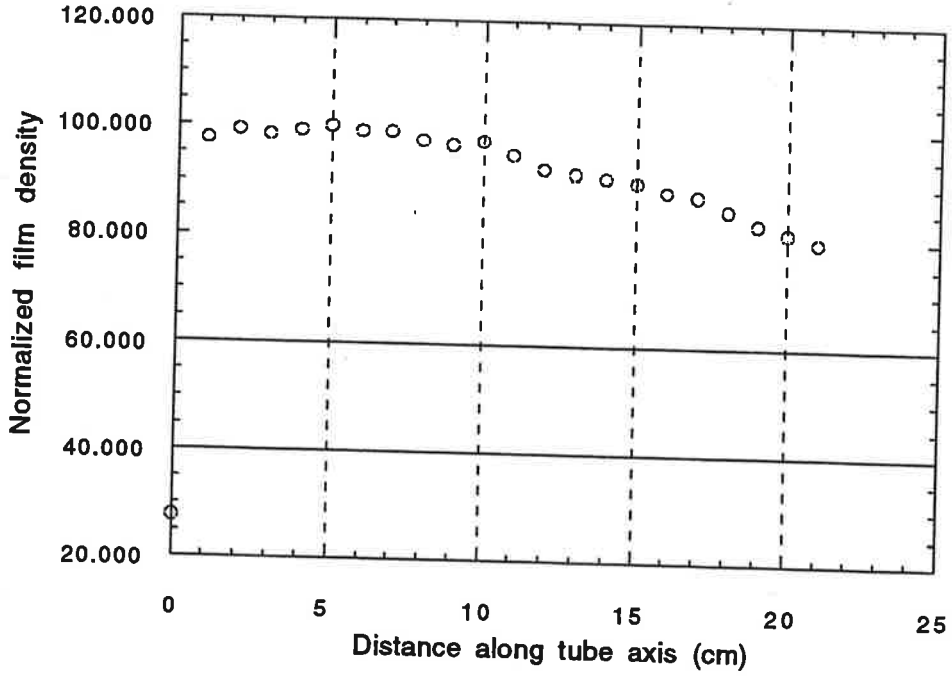
120.000
100.000
80.000
60.000
40.000
20.000
Normalized film density
0
5
10
15
20
25
Distance along tube axis (cm)

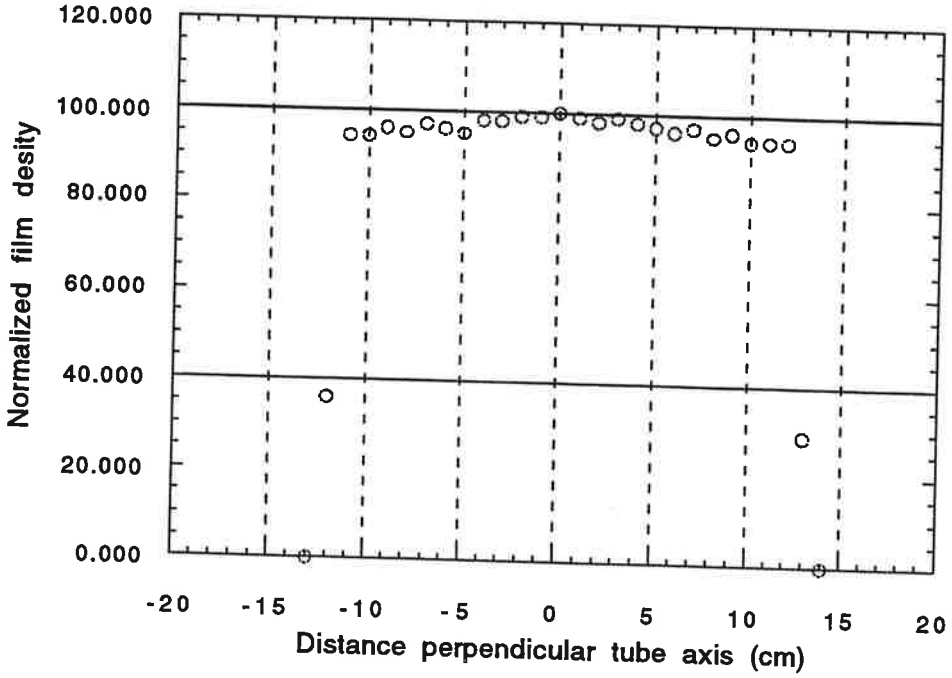
120.000
100.000
80.000
60.000
40.000
20.000
0.000
Normalized film desity
-20
-15
-10
-5
0
5
10
15
20
Distance perpendicular tube axis (cm)

Table 2.2 First and second half-value layers for the UW-ADCL molybdenum anode calibration beams.

	UW-ADCL @ 100 cm		
	HVL-1	**HVL-2**	**H.C.**
Beam code	**(mm Al)**	**(mm Al)**	**%**
Moly 23	0.307	0.384	79.9
Moly25	0.332	0.402	82.6
Moly28	0.366	0.438	83.6
Moly30	0.388	0.444	87.4
Moly35	0.410	0.505	81.2

2.4 Half Value Layer

The half value layer (HVL) of a beam is defined as the thickness of some standard material required to reduce the exposure of a beam to half its original value [2]. The HVL of a beam is considered an important beam characterization parameter for image quality, patient dose, and regulatory compliance. HVLs were measured in this study primarily to characterize the x-ray beam in which chamber calibrations were performed. An investigation was also made into the dependence of HVL determination on the energy dependence of an ionization chamber's response, these results are presented in Chapter 5, Section 6.

The errors in the measurement of half-value layer can be large depending on the equipment and the methods used to acquire the data. One source of uncertainty in HVL measurements result from the energy dependence of the detector used to measure the exposure. Wagner, Archer and Cerra [3] showed that severe energy dependence in the mammography range will result in significant errors in mammographic HVL measurement. Wagner and TG6 [4] suggest that a change in correction factor over the range of mammographic beam qualities (from about 20 to 50 kVp) should be less than 5% to ensure an adequately small, ±10%, error in the measurement of HVL. This accuracy is adequate to determine modest, 2 kVp, changes in beam quality, but will introduce significant uncertainty to the mean-glandular dose as will be discussed in Chapter 5, Section 7.

Half-value layers were measured on all the beams in this investigation. Experimental procedures followed the recommendations of Wagner, Archer and Cerra [2] to establish accuracy in HVL measurements to within ±10%. A set of high purity aluminum (>99.999% pure) filters was borrowed from the Accredited Dosimetry Calibration Laboratory at the M.D. Anderson Hospital, Houston, Texas. The thickness of each of these attenuators was determined by NIST. The UW-FAC with its flat energy response was employed for these measurements. A monitor chamber accounted for variations in tube output. For a source to detector distance of 1.00 m, the attenuation plates are positioned at

0.5 m. The HVL for each beam was determined using a semilogarithmic interpolation of neighboring data points that did not differ by more than 0.1 mm in aluminum filtration. The homogeneity coefficient, which is the ratio of first half-value-layer to the second half-value-layer and is a measure of the hardness of the photon beam, was also calculated for the x-ray beams. The uncertainty associated with these HVL measurements, including the day to day variations in the x-ray beams, were 1% for the tungsten beams and 3% for the molybdenum beams.

First and second HVLs were measured on the Philips orthovoltage system with the UW-FAC and the results are shown in Table 2.1 along with the HVL data for NIST beams. The FAC aperture was positioned at a distance of 1.0 m from tube focus (marked with a red dot on the side of the tube housing). Thin filters of high-purity aluminum were positioned perpendicular to the beam at about 50 cm from tube focus. Charge measurements were normalized to transmission monitor response.

HVLs were measured for the clinical mammography system with the UW-FAC and the high-purity aluminum attenuators following the same procedure as for the tungsten anode system and these results are shown in Table 2.2.

2.5 References

[1] P.J. Lamperti, T.P. Loftus and R. Loevinger, "Calibration of X-Ray and Gamma-Ray Measuring Instruments," NBS Special Publication 250-16 (1988).

[2] E. D. Trout, J. P. Kelley, and A. C. Lucas, "Determination of Half-Value Layer," Am. J. Roentgenol, **84**, 729-740 (1960).

[3] L. K. Wagner, B. R. Archer, and F. Cerra, "On the Measurement of Half-value Layer in Film-screen Mammography," Med. Phys. **17**, 989-997 (1990).

[4] L. K. Wagner, D. P. Fontenla, C. Kimme-Smith, L. N. Rothenberg, J. Shepard, and J. M. Boone, "Recommendations on performance characteristics of diagnostic exposure meters: Report of AAPM Diagnostic X-ray Imaging Task Group No. 6," Med. Phys. **19,** 231-241 (1992).

CHAPTER 3 SPECTRAL MEASUREMENTS

In diagnostic radiology, it is important to determine the x-ray spectrum accurately for the investigation of patient dose, image quality, comparison of imaging systems and the calibration of dosimeters with pronounced energy-dependent response. With the development of high-resolution semiconductor detectors with reasonably high detection efficiency and the accurate determination of the detector's energy response, accurate measurements of x-ray spectra can be made. The response of such detectors is well understood and involves primarily two mechanisms that cause the detected energy to be different than the incident photon energy: (a) the escape from the detector of characteristic x-rays resulting from photoelectric absorption events in the germanium K-shell and (b) the escape from the detector of the incident photons scattered to lower energies in Compton collisions. The effect of the K x-ray escape predominates for incident photon energies below ~100 keV and causes additional peaks in the pulse-height distribution displaced to energies lower than that of the incident photon by an amount equal to the energies of the germanium K x-rays. In most cases, the K x-ray escape probabilities are quite insensitive to the detector dimensions [1]. Corrections for these spurious detection effects can be arrived at either by direct means, analytic formulae or by Monte Carlo simulation [1 & 2].

A difficulty that must be overcome in the measurement of radiographic spectra is that the high fluence rate produced under imaging conditions may exceed the capabilities of the spectrometer system. Methods must be employed which reduce the photon fluence without distorting the measured spectra. Several methods of dealing with the high count rate problem have been suggested by various investigators. These methods include (a) large focal spot to detector distance [3]; (b) measurement of the Compton-scattered spectrum and derivation of the primary spectrum [4]; and (c) the use of collimators with small apertures [5]. This last method is simplest in its set -up and is the most commonly used.

The x-ray spectra that are presented in this work were measured to quantitatively characterize the differences between the clinical and calibration x-ray beams. The spectra provide a determination of first- and second-half-value-layers and peak accelerating potential on the x-ray tube, which can be compared with values measured by other techniques. The spectra also are used as input into the monte carlo code to enable accurate calculation of the scattered photon correction to the free-air chamber exposure measurements.

3.1 Description of Spectrometer System

The photon spectral measurement system featured a high purity (intrinsic) germanium (HPGe) detector (model 1113-10220 s/n B-18) from the GLP Low-Energy Photon Spectrometer series (Ortec Inc., Oak Ridge, TN). The detector element was a p-type planar crystal 10 mm diameter with a thin, ion-implanted front contact. The crystal was mounted in a cryostat consisting of a vacuum chamber thermally coupled to a liquid nitrogen heat sink (MVE Cryogenics dewar model AL-30 s/n 2428-B). The outer vacuum jacket was constructed with a 25.4 μm thick beryllium entrance window to maximize the system's low energy efficiency. The detector face was located 10 mm from the inside wall of the entrance window. The system's quoted "useful" energy range is 3 keV to 300 keV. A bias voltage of negative 1400 volts was applied to the crystal during accumulation of pulse height spectrum by an Ortec power supply (model 456H s/n 434). The data from the preamplifier (Ortec 117B s/n 688), which was permanently attached to the crystal, were sent to a Canberra amplifier (model DB-2) and then to the Inotech 5200 (s/n B108151) analog to digital converter (ADC). After a spectrum was collected, the data were dumped to an IBM computer (via RS-232) and ST240 terminal emulation software.

The data output from a multi-channel analyzer (MCA) is simply counts per channel which must be converted into an x-ray energy spectrum. For the conversion to be accurate, the linearity and energy calibration of the spectrometer system must be determined.

3.2 Spectrometer System Calibration

The linearity of the ADC was checked with a pulser (DB-2). Pulses of different amounts of charge were provided via an internal voltage divider. The pulse data were fit versus channel number with linear regression and data were linear to r = 0.99998. The zero on the ADC was adjusted until the pulser data fit intersected near channel zero (data fit intersected to channel = 0.53).

To determine the channel to energy conversion for the detector crystal and MCA combination pulse height data were acquired using radiation sources with gamma-decay energies covering the energy range of interest. Calibration sources of Am-241, Fe-55 and Ba-133 were used in this work; the gamma ray energies of these sources are listed in Table 3.1. Each source was placed immediately in front of the white plastic protective cover of the thin Be window. The counting times for these sources were 5×10^3 seconds. A background spectrum was collected for a period of 10^4 seconds and is shown in Figure 3.1. Background was prorated to the collection time of the energy calibration spectrum and subtracted from each raw spectrum. The background corrected barium, iron and americium data are shown in Fig. 3.2.

The peak channel of each gamma ray was determined from the background corrected data and plotted versus gamma ray energy in Figure 3.3. A linear regression analysis of these data yields

$$\text{Energy} = 0.22376 + 0.10068 * \text{Channel}$$

with a correlation coefficient of 0.99997. This curve-fit was then used to convert the channel number to photon energy in keV.

Table 3.1: Gamma-decay sources used to calibrate energy to channel number for HPGe detector system.

Radionuclide	Energy (keV)	% emission	bin#
Am-241	13.9	0.427	137
	26.345	0.024	264
	33.205	0.001	333
	59.537	0.359	598
	69.231	0.002	--
Fe-55	0.64	0.004	--
	5.888	0.082	54
	5.899	0.163	54
	6.490	0.033	--
Ba-133	4.290	0.168	--
	30.625	0.342	310
	30.973	0.634	310
	35.000	0.228	352
	53.155	0.0214	535
	79.621	0.0255	795
	80.997	0.033	808

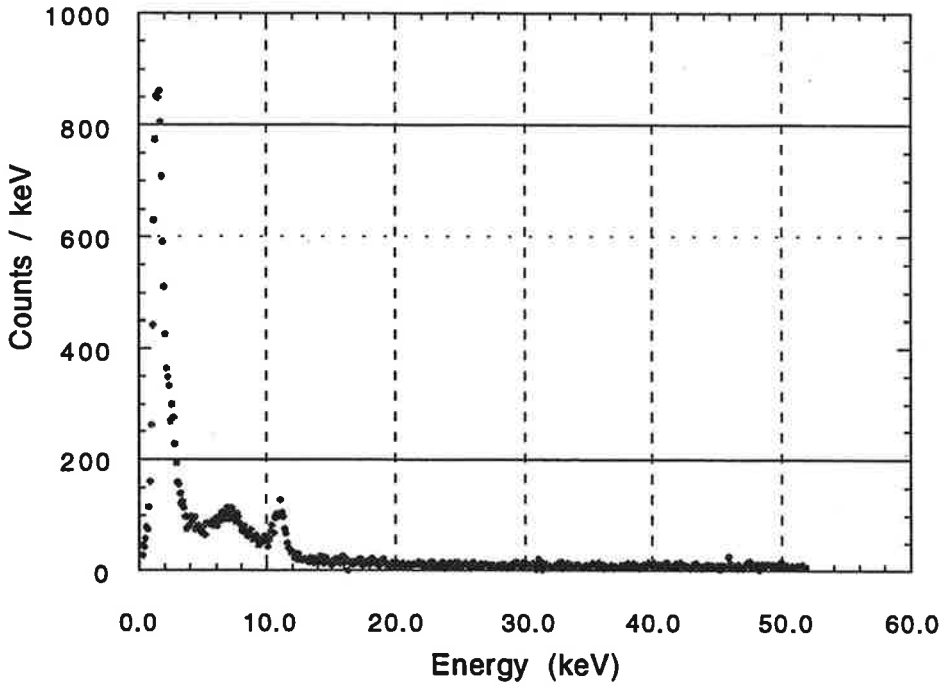

Figure 3.1 Background spectrum collected for 10^4 seconds for HPGe spectrometer system.

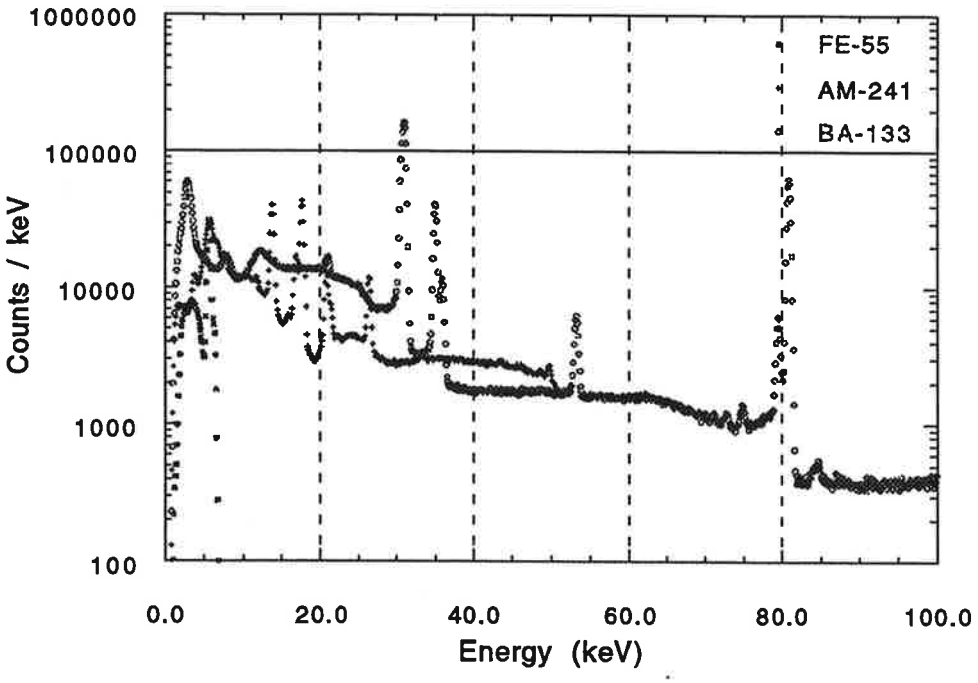

Figure 3.2 Background corrected barium, iron and americium data used to calibrate HPGe system.

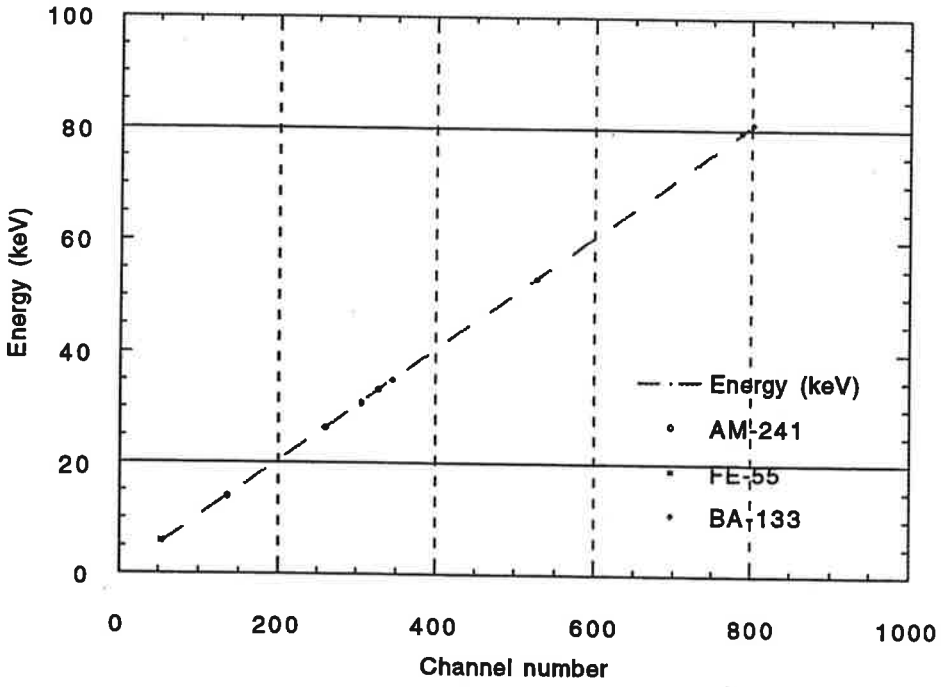

Figure 3.3 Peak channel versus gamma energy for calibration sources.

3.3 Fluence Reduction

A major problem when using energy dispersive detectors is the limited count rate accepted by the detector for accurate performance. It is therefore impossible to measure energy spectra of the primary beam under normal operating conditions which has on the order of 10^8 photons/cm^2/sec. The photon fluence rate at the detector must be reduced. Ideally, such a reduction should be uniform over the entire photon energy range and the detector system should have high, or at least uniform, detection efficiency over this energy range.

A straightforward method of reducing the number of photons reaching the detector is to reduce the solid angle subtended by the detector. This can be accomplished by employing large distances between the detector and the x-ray tube focus and very small collimator openings in front of the detector. The molybdenum spectrum were collected at 1.0 m from the tube focus. A lead pinhole holder with diameter of 5 mm was placed immediately in front of the detector to further reduce the photon fluence. The tungsten spectrum were also collected at a distance of 1.0 m with a smaller 1.5 mm diameter lead aperture placed immediately in front of the detector.

To further reduce the photon fluence of the clinical molybdenum system, the filament control voltage was minimized, thereby minimizing the tube current. Power resistors were added in series to the high tension side of the transformer to increase the load and maintain a stable kV. During data collection, the kVp was monitored on the calibrated voltage divider readout.

3.4 Spectral measurements

Molybdenum spectra were collected for 25, 28, 30, 35 and 40 kVp. Spectra were collected for 100, 200 or 300 seconds depending on the kVp which inherently controlled the mAs. Count rates were on the order of 1600 counts per second with dead time losses less

than 5%. Tungsten x-ray spectra were collected in the same geometry for beam energies between 20 and 50 kVp with nominal tube current of 0.00 mA (minimal electron current through x-ray tube). Data were collected over 300 seconds at a count rate of 250 counts per second and dead time losses less than 3%. Spectra were also collected at 30 kVp with the transmission monitor removed from the beam.

3.5 Data Correction

Once spectral data are collected, the next requirement for determining the true spectrum from the raw data is to correct the measured spectrum for spurious detector effects. Spurious effects are due to radiation that escapes from the detector or is backscattered into it. These effects include the escape of K-fluorescence and Compton photons from the detector, the detector's efficiency as a function of energy and collimation effects. The K-edge for Ge is 11.103 keV and can result in the photon's energy not being totally absorbed in the detector. A false energy peak can be produced from a photoelectric interaction between this photon and a K-shell electron. Also, the Be window above the vacuum housing on the detector will produce a loss of efficiency below 10 keV.

Corrections were made for these detector distortions using a Quick Basic code provided by Tom Fewell of FDA/CDRH [6]. The code used germanium detector efficiency data calculated by Seltzer [1]. The loss of efficiency below the Ge K-edge (11.103 keV) is due to the interaction of x rays with the entrance window and is calculated using the attenuation coefficient of beryllium. The loss of efficiency between 11.103 keV and 50 keV is due to the escape of Ge K x rays from the detector. The Compton process is small in this region, but corrections were applied using Doi's Compton technique [7].

The simplest way to correct a measured spectrum is to divide the measured photon counts in a given channel by the photopeak efficiency at the same energy. A more advanced correction technique accounts for the K-escape radiation loss as well as the photopeak

efficiency correction. This method was used to correct these spectral data. The photopeak efficiency correction begins at the maximum energy of the measured spectrum; the K-escape fraction for that particular energy is then multiplied by the corresponding number of counts and subtracted from the number of counts in the channel whose energy is equal to that less the K-fluorescence energy.

The correction of spectra for the distortion due to the Compton effect is more difficult because the distribution of escaped Compton scattered photons is complicated and depends on energy. The correction method is then similar to that used for the K-escape correction, except that the Compton fraction of photons is subtracted from the low-energy channels as a rectangular distribution.

3.6 Data Analysis

The corrected photon energy spectral data for the tungsten anode x-ray system are shown plotted in Figures 3.4 - 3.9 and the molybdenum anode spectra are shown in Figures 3.10-3.14. Figure 3.4 also includes the measured data to help quantify the magnitude of the corrections applied to arrive at the corrected fluence spectra. For the tungsten spectra, no photons are present below about 6 keV due to the 2 mm Be exit window of the x-ray tube plus the additional aluminum added to match NIST beams. Figue 3.11 shows the data for the ADCL 28 kVp molybdenum anode beam compared with data from Jennings [8] of the Food and Drug Administration, Center for Devices and Radiological Health. The molybdenum spectra are also sharply attenuated below about 8 keV due to the 1 mm Be tube window plus the 30 mm of added molybdenum filtration. The peaks present in the tungsten spectra at 9.5 and 11 keV are due to the L-beta (9.67 keV) and L-gamma (11.283 keV) of tungsten, while the peak at 8 keV appears to be a combination of the copper K-alpha (8.047 and 8.027 keV) and the tungsten L-alpha (8.33 and 8.396 keV). The peaks at 17.5 and 19.5 keV in the molybdenum spectra are the characteristic K-alpha (17.48 and 17.37 keV)

and K-beta (19.61 and 19.96 keV) of molybdenum [9]. The drastic reduction in photons above 20 keV in the molybdenum spectra are due to the K-shell absorption edge of the added molybdenum filtration.

Spectra were collected for the UW-ADCL 30-M beam with and without the transmission monitor in the beam to investigate the attenuation of the beam by the chamber windows. A plot of the chamber transmission, spectra with chamber divided by spectra without chamber, is shown in Figure 3.15. Down to about 15 keV the chamber permits nearly all photons to pass through and over 80% transmission down to 7 keV. Note that at 29.2 keV the transmission shows a sharp decline due to the K-edge of the tin which comprises the chamber windows.

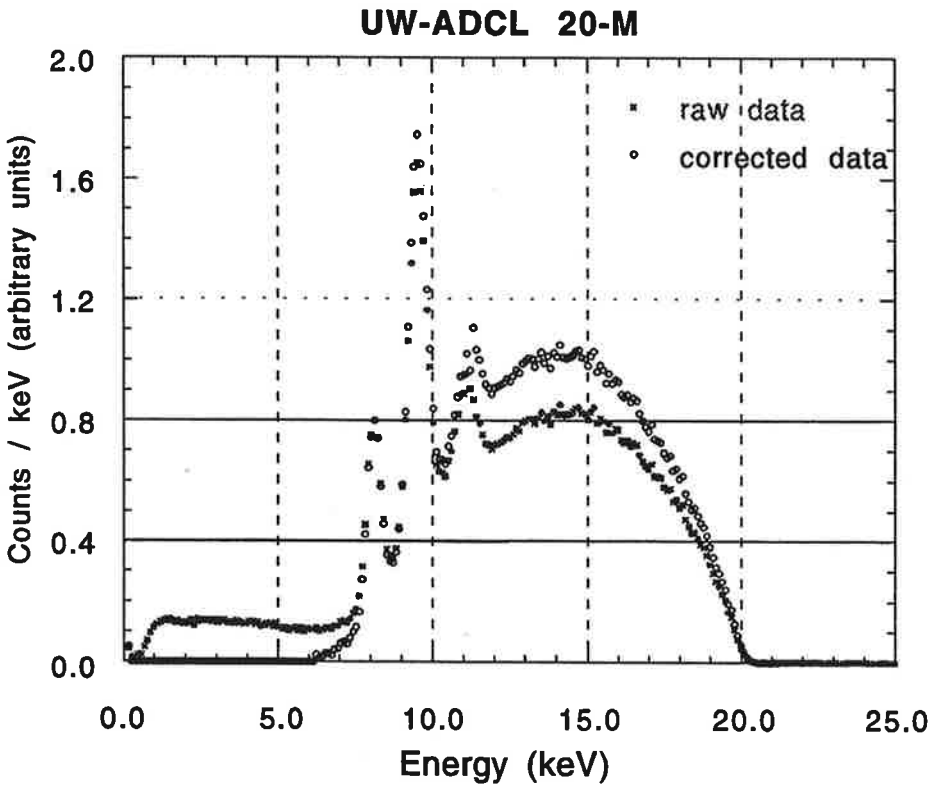

Figure 3.4: Measured and corrected photon energy spectrum for UW-ADCL tungsten anode 20-M x-ray beam.

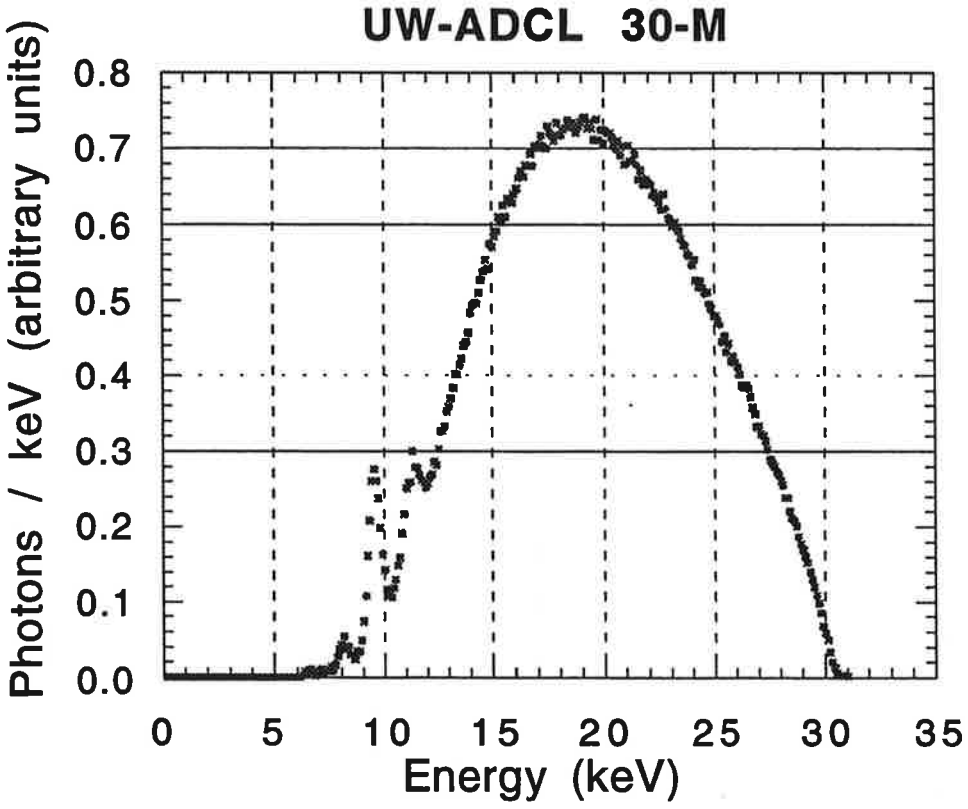

Figure 3.5: Corrected photon energy spectrum for UW-ADCL tungsten anode 30-M x-ray beam.

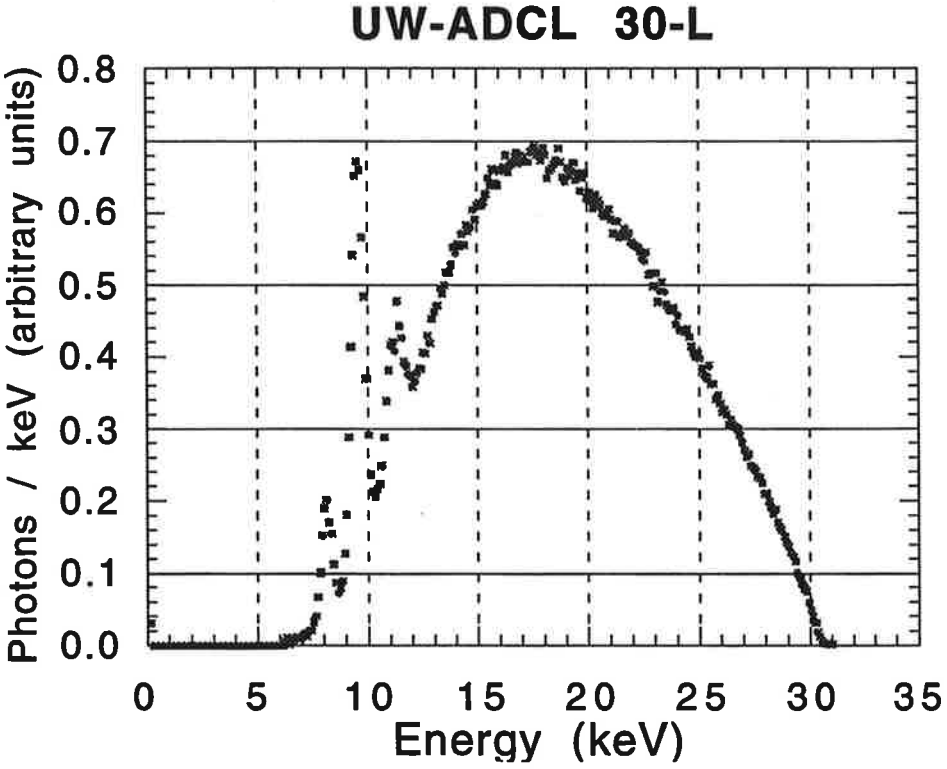

Figure 3.6: Corrected photon energy spectrum for UW-ADCL tungsten anode 30-L x-ray beam.

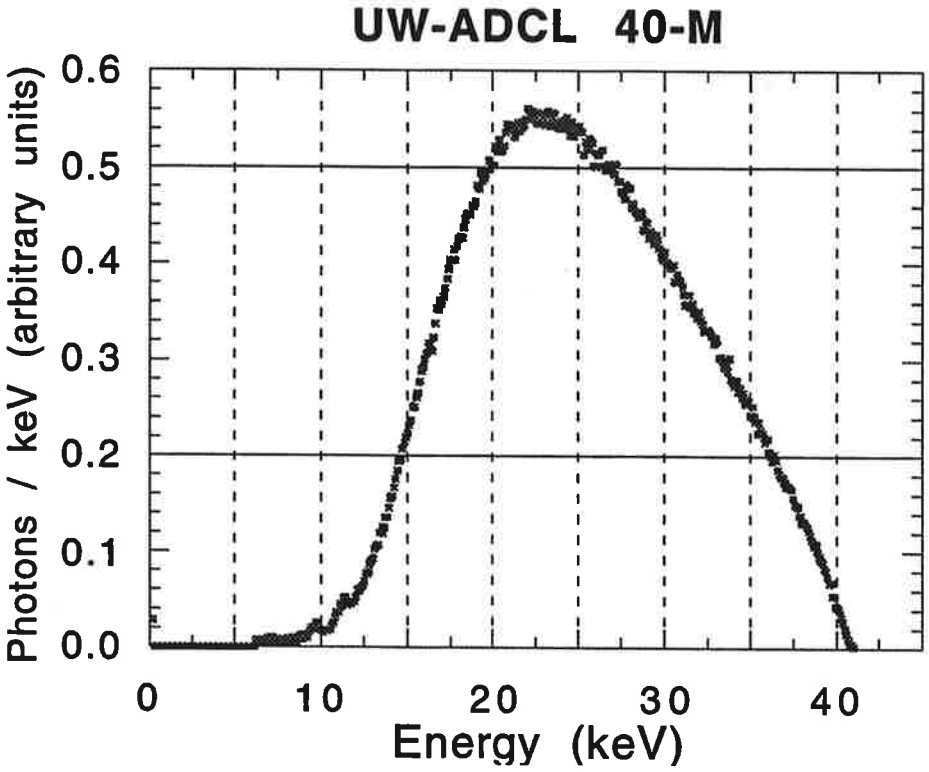

Figure 3.7: Corrected photon energy spectrum for UW-ADCL tungsten anode 40-M x-ray beam.

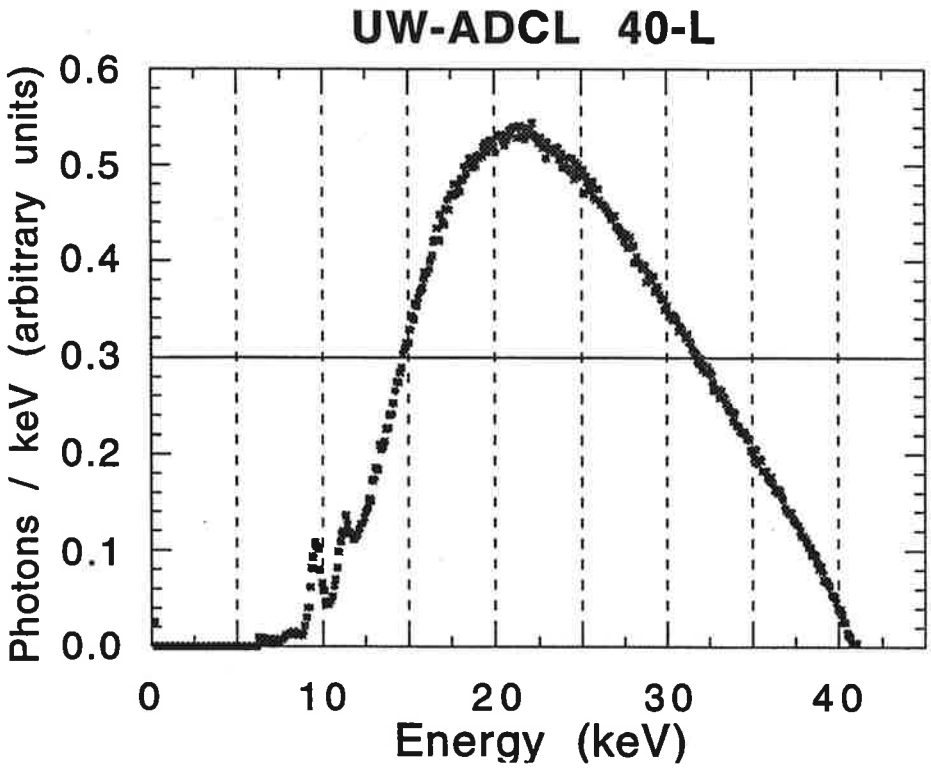

Figure 3.8: Corrected photon energy spectrum for UW-ADCL tungsten anode 40-L x-ray beam.

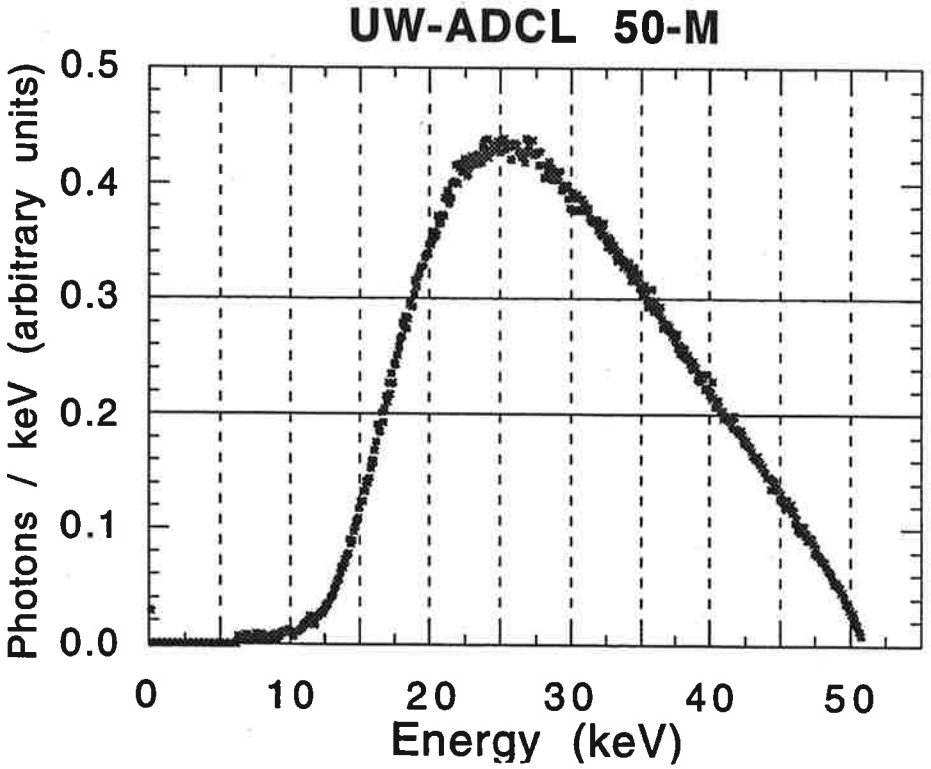

Figure 3.9: Corrected photon energy spectrum for UW-ADCL tungsten anode 50-M x-ray beam.

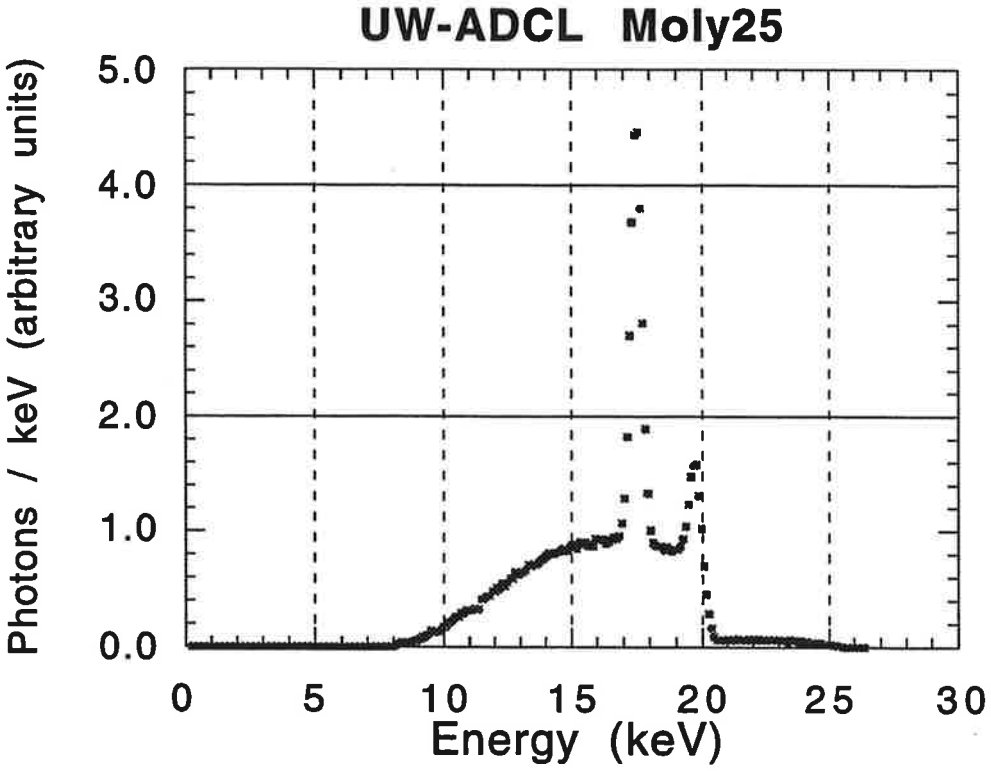

Figure 3.10: Corrected photon energy spectrum for UW-ADCL Moly 25 x-ray beam.

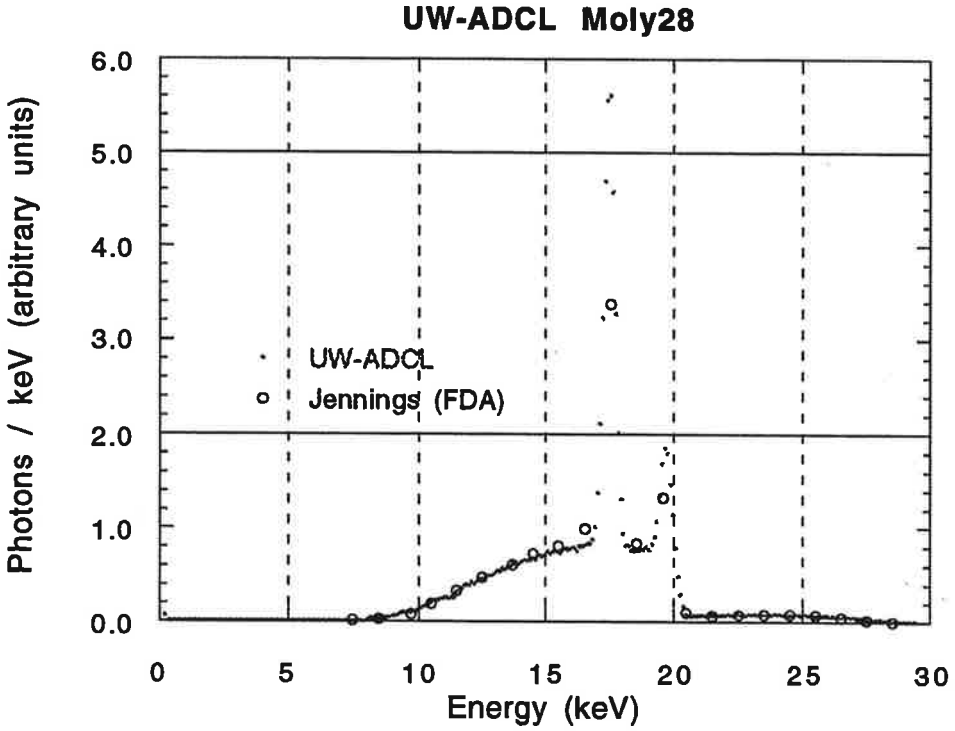

Figure 3.11: Corrected photon energy spectrum for UW-ADCL Moly 28 x-ray beam compared with FDA Moly anode 28 kVp spectrum data.

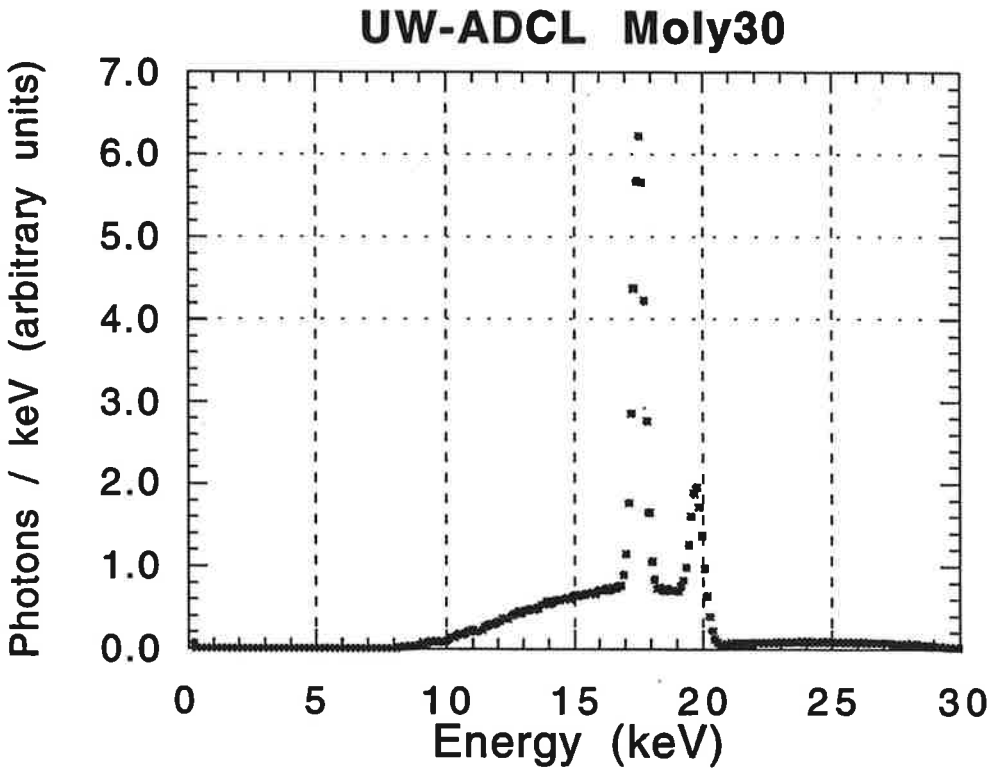

Figure 3.12: Corrected photon energy spectrum for UW-ADCLMoly 30 x-ray beam.

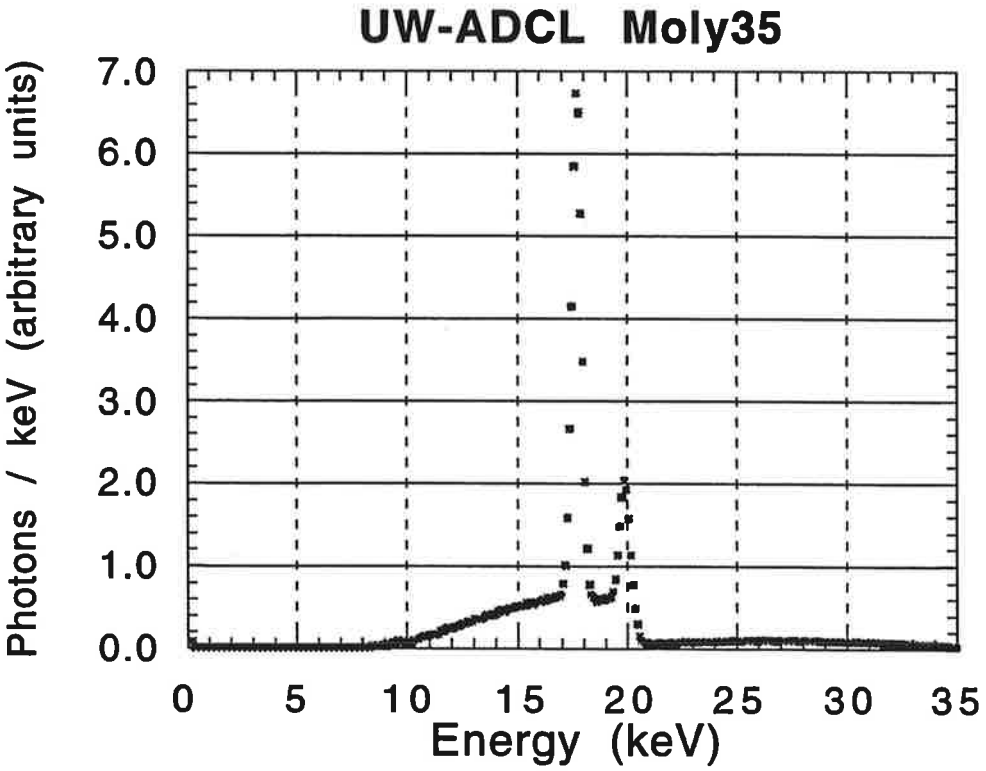

Figure 3.13: Corrected photon energy spectrum for UW-ADCL Moly 35 x-ray beam.

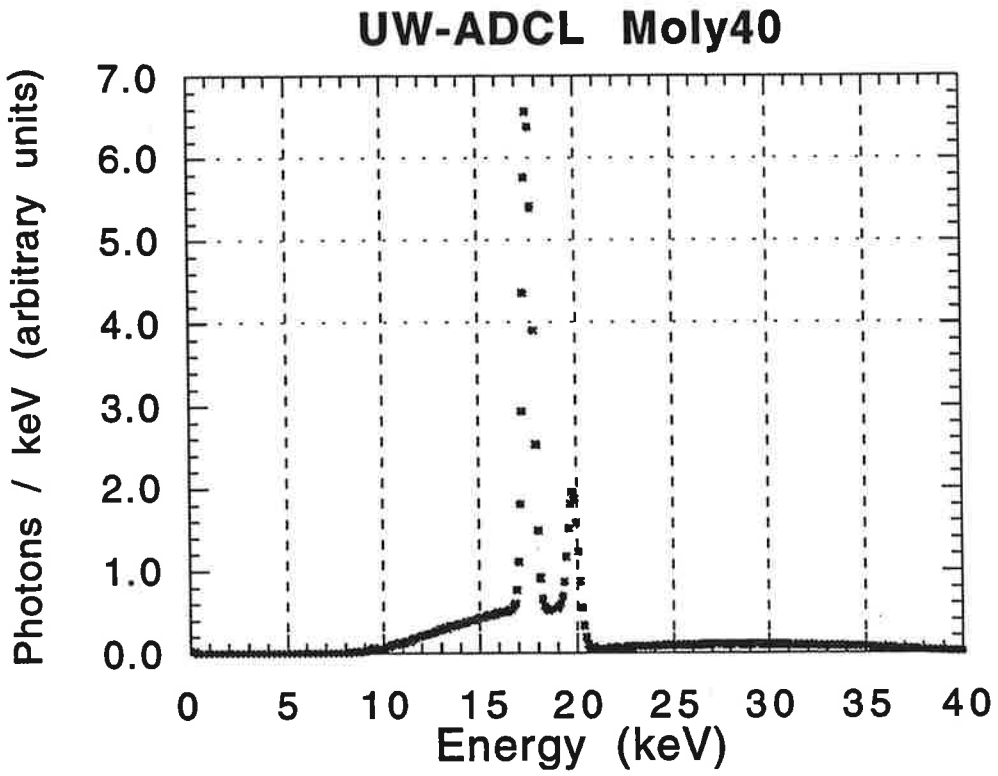

Figure 3.14: Corrected photon energy spectrum for UW-ADCL Moly 40 x-ray beam.

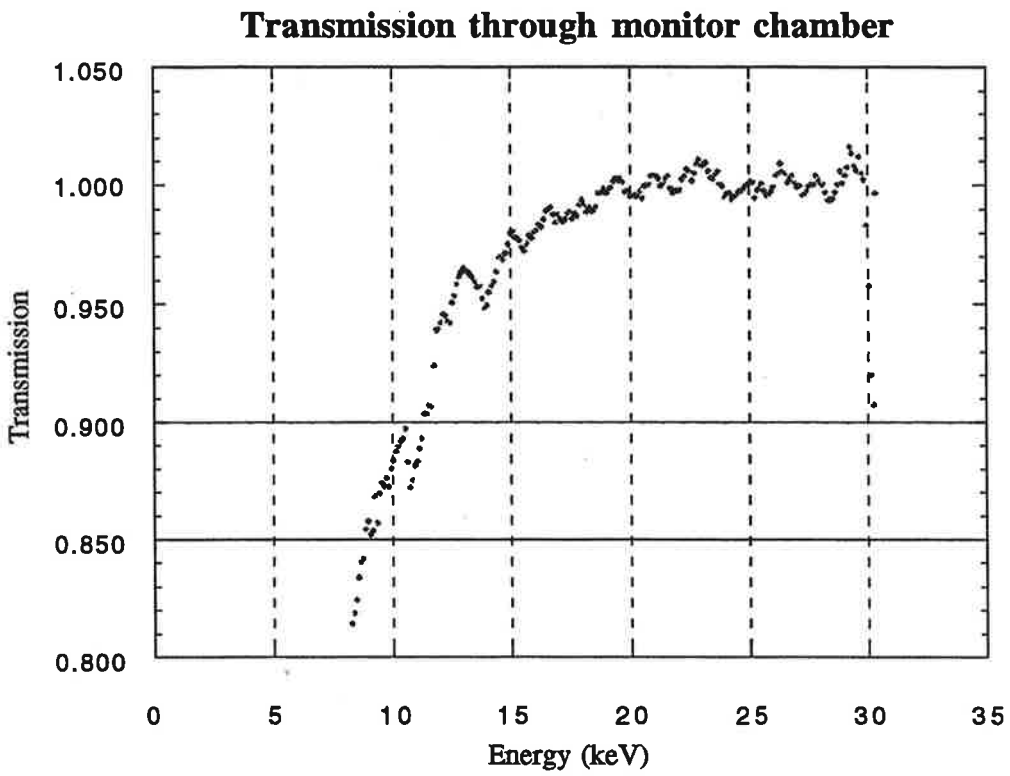

Figure 3.15 Plot of transmission through parallel-plate transmission monitor for UW-ADCL 30-M tungsten anode x-ray beam.

3.7 Calculated HVL

The half-value layer in aluminum of each of the calibration beams were calculated from the corrected photon energy spectra. As previously described, the half-value layer of a beam is defined as the thickness of some standard material required to reduce the exposure of a beam to half its original value. The HVL in aluminum can therefore be calculated from the beam spectrum as follows:

$$\frac{\sum_{E=0}^{kVp} E \bullet \left[\frac{\mu_{en}}{\rho}\right]_{E,air} \bullet \phi \bullet \exp\left[-\left[\frac{\mu_{att}}{\rho}\right]_{E,Al} \bullet \rho \bullet HVL\right]}{\sum_{E=0}^{kVp} E \bullet \left[\frac{\mu_{en}}{\rho}\right]_{E,air} \bullet \phi} = 0.5$$

where E is the photon energy in each bin, $[\mu_{en}/\rho]_{E,\,air}$ is the mass energy-absorption coefficient of air at each bin energy, φ is the measured photon fluence, $[\mu_{attn}/\rho]_{E,Al}$ is the mass attenuation coefficient for aluminum at each bin energy in $[cm^2/g]$, ρ is the mass density of aluminum in $[g/cm^3]$ and HVL is the half-value layer in cm of aluminum. The mass energy-absorption coefficients for air and mass attenuation coefficient for aluminum were calculated from polynomial fits by Tucker et al. [10] to data tabulated by Hubble [11].

The mass attenuation coefficient includes both the probability of the attenuation of primary photons and the scattering of photons out of the primary beam. Calculation of HVL from the corrected spectra using the total interaction coefficient assumes narrow beam geometry, where all of the scattered photons are eliminated from the detected beam. HVL calculations performed with the total attenuation coefficient minus the probability of coherent scatter assumes broad beam approximation. The accuracy of these HVL calculations must take into account the accuracy of the measured photon energy spectra as well as the accuracy of the attenuation coefficient data. The largest source of uncertainty would be that associated

Table 3.2: Half-value layers calculated from corrected photon energy spectrum compared with measured values.

	measured with FAC	calculated from spectra, narrow beam geometry		calculated from spectra, broad beam geometry		monte carlo calculation	
Beam code	**HVL (mm Al)**	**HVL (mm Al)**	**Δ% HVL**	**HVL (mm Al)**	**Δ% HVL**	**HVL (mm Al)**	**Δ% HVL**
20-M	0.147	0.138	-6.1	0.142	-3.4		
30-M	0.369	0.347	-6.0	0.364	-1.4	0.37	+0.3
40-M	0.773	0.693	-10.3	0.738	-4.5		
50-M	1.062	0.938	-11.7	1.011	-4.8		
30-L	0.264	0.239	-9.5	0.249	-5.7		
40-L	0.524	0.509	-2.9	0.541	+3.2		
Moly 25	0.307	0.290	-5.5	0.303	-1.3		
Moly 28	0.332	0.317	-4.5	0.333	+0.3		
Moly 30	0.366	0.336	-8.2	0.353	-3.6	0.33	-9.9
Moly 35	0.388	0.374	-3.6	0.394	+1.5		
Moly 40	0.410	0.393	-4.1	0.414	+1.0		

with the spectra which depends on the corrections applied for K-fluorescence and Compton photon escape, efficiency of the detector and the detectors energy versus channel calibration. Error analysis assigns an uncertainty of ±4% to the HVLs determined by these calculations.

The HVLs for two of the calibration beams were determined by monte carlo calculation. The corrected photon spectra for the tungsten 30 kVp and the molybdenum 30 kVp beams were transported through the free-air chamber geometry as described in Appendix A. Aluminum sheets 10 cm square were added midway between the photon source and the chamber aperture. Thicknesses were adjusted until the calculated dose was halved. The HVLs as calculated by the monte carlo code also rely on the accuracy of the measured spectra and the interaction coefficient data, plus the statistical uncertainty from the simulation, which is ±3.5% for these calculations. Therefore the uncertainty in the calculation of HVLs is ±5.5%.

The calculated half-value layers, with and without contribution of coherent scattering, along with the values calculated via monte carlo simulation are given in Table 3.2 and these data are compared with data measured with the free-air chamber.

Also determined from the HVL are the x-ray beam effective energy and linear attenuation coefficient in air. These data are compared with the linear attenuation coefficients measured with the free-air chamber in Table 3.3.

Table 3.3: Effective photon energy and linear attenuation coefficients determined from measured photon energy spectrum compared with values measured with free-air chamber.

UW-ADCL Beam code	measured with FAC μ_{air} (cm^2/g)	calculated from spectra Effective Energy (keV)	μ_{air} (cm^2/g)	Δ% for μ_{air}
20-M	4.49	11.2	4.30	-4.2
30-M	1.91	15.2	1.83	-4.2
40-M	1.057	19.5	0.978	-7.5
50-M	0.871	21.7	0.769	-11.7
30-L	2.81	13.5	2.53	-11.2
40-L	1.59	17.5	1.27	-20.1
Moly 25	2.5	14.4	2.11	-15.6
Moly 28	2.16	14.8	1.96	-9.3
Moly 30	2.17	15.1	1.86	-14.3
Moly 35	1.85	15.7	1.68	-9.2
Moly 40		15.9	1.63	

3.8 References

[1] S. M. Seltzer, "Calculated Response of Intrinsic Germanium Detectors to Narrow Beams of Photons with Energies up to ~300 keV," Nuclear Instruments and Methods **188**, 133-151 (1981).

[2] C. S. Chen, K. Doi, C. Vyborny, H. P. Chan and G. Holje, "Monte Carlo simulation studies of detectors used in the measurement of diagnostic x-ray spectra," Med. Phys. **7**, 627-635 (1980)

[3] E. Storm and D. W. Lier, "X-Ray Spectrum Distributions in Roentgens," Health Physics **23**, 73 (1972).

[4] T. R. Fewell and K. E. Weaver, "The measurement of diagnostic x-ray spectra with a high purity germanium spectrometer," Proc. SPIE **56**, 4 (1975).

[5] H-P Chan, Ph.D. dissertation University of Chicago, USA (1981).

[6] T. R. Fewell and R. E. Shuping, "Photon energy distribution of some typical diagnostic x-ray beams," Med. Phys. **4**, 187-197 (1977).

[7] H-P Chan and K.Doi, "Physical Characteristics of scatter radiation in diagnostic radiology; Monte Carlo simulation studies," Med. Phys. **12**, 152-165 (1985).

[8] R.J. Jennings, private communication, Food and Drug Administration, Center for Devices and Radiological Health, Rockville, MD (1994).

[9] R. C. Weast, ed., *CRC Handbook of Chemistry and Physics*, 66th ed., (CRC Press, Boca Raton, Fl, 1985).

[10] D. M. Tucker, G. T. Barnes, and X. Wu, "Molybdenum target x-ray spectra: A semiempirical model," Med. Phys. 18, 402-407 (1991).

[11] J. H. Hubble, "Photon mass attenuation and energy-absorption coefficients for 1 keV to 20 MeV," Int. J. Appl. Radiat. Isot. 33, 1269-1290 (1982).

CHAPTER 4 FREE-AIR IONIZATION CHAMBERS

The use of x-rays in medicine and biology requires the measurement of exposure, which is a measure of the energy transfer of x-rays in air. This in-air measurement can then be converted to a patient dose by multiplication by a number of conversion factors. The definition of exposure requires the measurement of all ionization produced by collision interactions in air by all electrons resulting from x-ray interactions in a known mass of air [1]. The Systeme International (SI) unit of exposure is the coulomb per kilogram (C/ kg); the special unit of exposure, the roentgen (R), is equal to 2.58×10^{-4} C/kg exactly. A free-air ionization chamber is an ionization chamber with air walls that are thicker than the range of secondary electrons that are created by the x-ray beam, therefore meeting the requirement of the definition of exposure. At mammography energies (23-35 kVp) the range of the secondary electrons in air is only a few centimeters. Therefore a chamber of practical size can be designed to collect all such secondary electrons and measure the absolute in-air exposure.

A number of different designs of free-air ionization chambers have evolved, some plane-parallel and some cylindrical in geometry. In a conventional parallel-plate free-air chamber, a diaphragm aligned with the beam axis at the front of the chamber passes a beam of cross-sectional area A_0 through the chamber. The plate system inside the chamber consists of three coplanar plates on one side of the beam and a parallel high-voltage plate opposite. The plates are parallel to the x-ray beam axis and equidistant from it. To provide a uniform electric field between the plates, a set of metal strips or wires encircles the space between them at both ends and at the top and bottom. These plates are electrically biased in uniform steps to establish parallel equipotential planes between the plates and to assist in producing electric field uniformity. The air volume in which the ionization is collected is

defined by the diaphragm area and the length, L, of the collecting electrode. If the lines of the electric field were perpendicular to both electrodes the air volume would be $V = A_0 \cdot L$. Since in practice electrical field distortion is present, it is necessary to introduce a correction factor to take into account any residual field distortion effect. A more important correction at the low energies encountered in mammography is the correction for the attenuation of the x-ray beam between the collector center and the defining plane of the entrance aperture. The linear attenuation coefficient at 20 keV in air is $\sim 10^{-3}$/cm and accounts for a correction of about 2%.

In 1961 Attix suggested the design of a variable-length free-air ionization chamber which differs in both geometry and operation from parallel-plate free-air chambers [2]. The chamber is cylindrical in design with an off-center collecting rod. The measurement procedure is based on a subtraction method: ionization measurements are taken at different plate separations and the difference is used to determine the x-ray exposure. The variable-length design also allows for the direct measurement of the significant air attenuation correction. The plate separations are accurately determined through the use of a precision screw. As a result of the measurement procedure, this chamber does not require a correction for field inhomogeneity since the effect of the unknown electric field lines near the chamber ends is constant and is eliminated by subtraction. Consequently, this chamber has no need for guard plates or other field shaping electrodes which are typical of conventional free-air chambers. Laitano and Toni describe the use of this type of free-air chamber as a national x-ray standard for 100 to 250 kVp x-ray beams [3]. In 1989 C. Meger et al.[4], here at the UW, designed and constructed such an ionization chamber for dosimetry applications of synchrotron produced ultrasoft x-rays. The design has been revised for mammography energy applications and improved with the independent control of plate separation and chamber position accomplished with two stepping motor controlled translation stages[5].

4.1 NIST Ritz Free-Air Ionization Chamber

The NIST 20-100 kV free-air chamber known as the Ritz chamber is shown in Figure 4.1. It is a parallel-plate chamber consisting of three collecting plates and a system of guard strips, all of which were constructed to minimize electric field distortion. The collector and guard plates were machined as a unit until they were coplanar to 2.5 μm. The plate separation is 90 mm with the three collectors of length 10, 30 and 70 mm. The plates are all parallel to the x-ray beam axis and equidistant from it. The distance of the plates from the beam is designed such that in the mammography energy region they are beyond the range of all the secondary electrons originating in the beam. The plate system is housed in a lead-lined steel box to exclude scattered x-rays from the collecting region. The defining plane of the tungsten alloy diaphragm, the point at which the exposure is determined, is located inside the box. Details of the NIST 20-100 kVp standard instrument are given in Ritz's original paper [6].

4.2 UW Attix Free-Air Ionization Chamber

The UW Attix free-air ionization chamber is designed for x-ray energies up to 50 kVp and is shown in Figure 4.2. An aluminum cylinder (89 mm inside diameter, 250 mm length) and two aluminum plates form a variable collecting volume. Aluminum, a low atomic number material, was chosen so that ionization due to scattered x-ray interactions will not be enhanced by the photoelectric effect. The cylinder and plates are attached to two stepping motor controlled translation stages. One stage is mounted on top of and parallel to the other enabling the independent control of plate separation and chamber position.

The x-ray beam is defined by an aperture of known area in a fixed diaphragm aligned with the chamber axis. The aperture is at least ten half-value layers thick to ensure minimal transmission of the primary beam. The apertures were fabricated from brass cylinder 15 mm

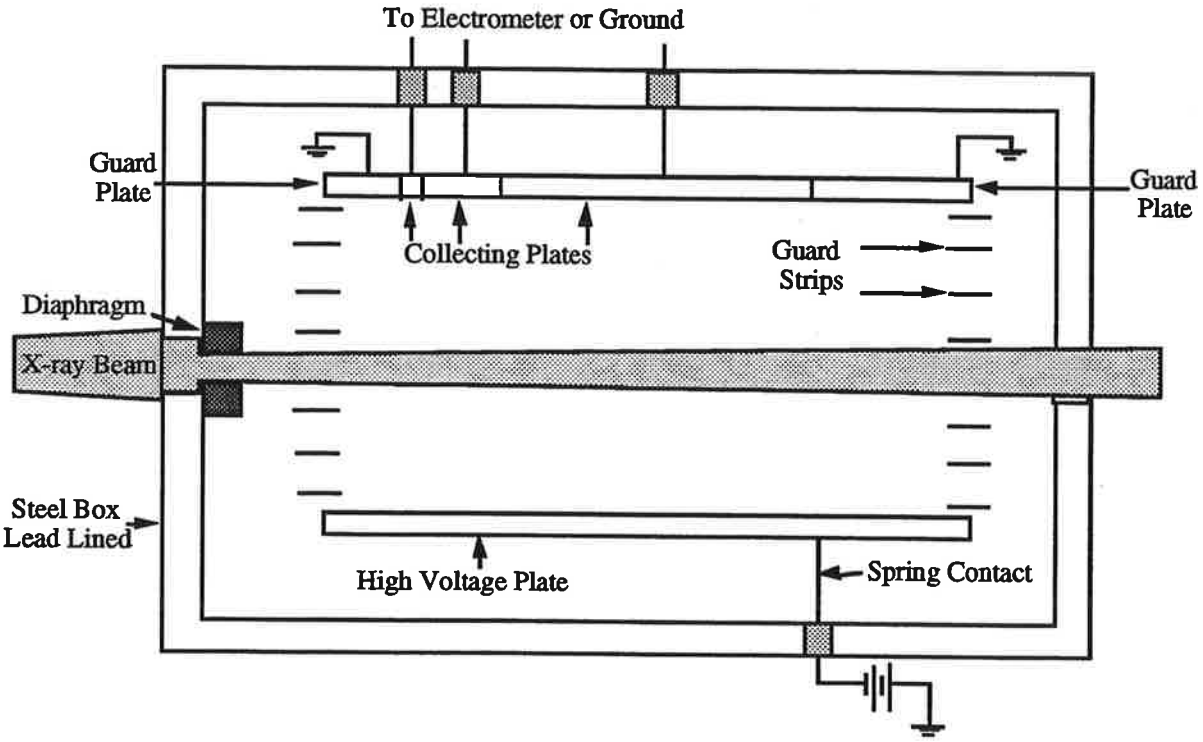

Figure 4.1: Sectional view of the NIST Ritz 20-100 kV parallel-plate free-air ionization chamber.

long and 26 mm diameter. Apertures were machined to diameters of 5, 7.5 and 10 mm.

The entrance and exit windows (free air) are 20 mm in diameter. The 44.5 mm radius of the chamber ensures that none of the secondary electrons originating in the mammography energy x-ray beam from collision interactions can reach the chamber wall. The minimum plate separation should be at least one radius to avoid secondary electrons from reaching the walls before losing all their energy. All energy of all secondary electrons that are created must be transferred within the chamber's volume to satisfy the definition of exposure.

The collecting rod is a 1.575 mm diameter stainless steel rod positioned approximately midway between central axis of the chamber and the chamber wall. Stainless steel was chosen for its accurately known and uniform diameter and its smooth finish which permits it to easily slide through the Teflon insulating bushing in the back wall as the plate separation is varied. The collector is held at ground potential. The small diameter ensures a small loss of ionization from electrons striking the collecting rod, but is sufficiently large so as to not create such a high electric field to permit gas multiplication of the ionization. The front end of the collector passes through an insulating bushing in the front wall and connects via coaxial cable to the electrometer. To the rear, the rod projects out of the collecting volume and into a grounded electrostatic shield. Both the front and back-end insulators of the collecting rod are made of Teflon and are provided with a grounded guard ring to eliminate the leakage of current across the insulator to the rod.

4.3 Ionization Measurement

The exposure rate is measured at the defining plane of the chamber diaphragm. This is possible since the beam divergence beyond the aperture is exactly compensated for by $1/r^2$ and can therefore be replaced, for purposes of calculation, by a parallel beam having the

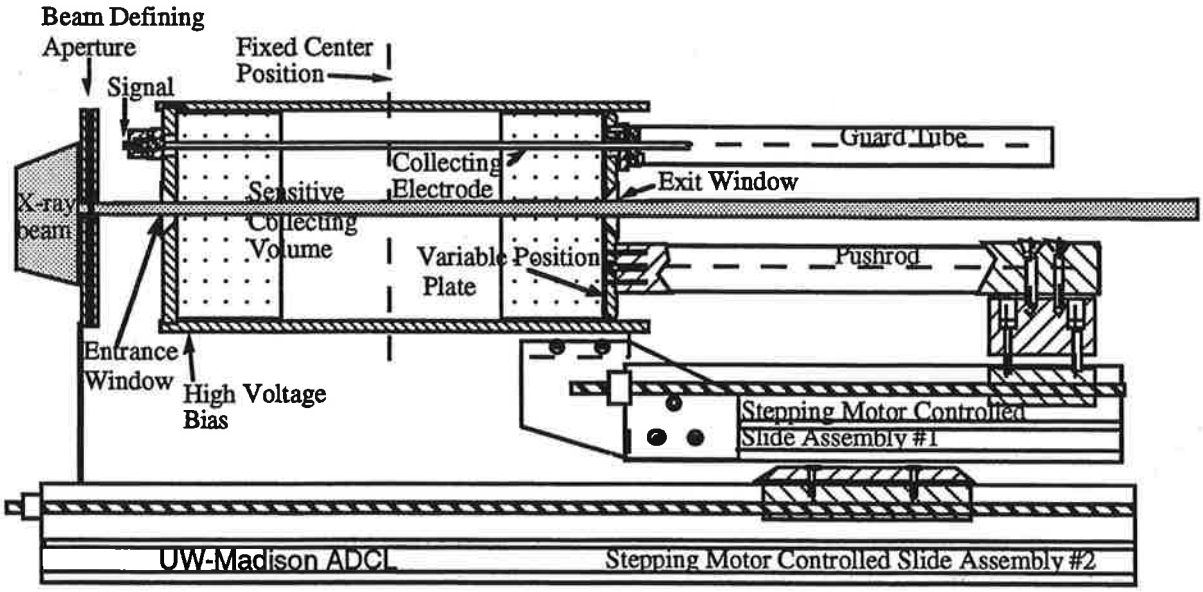

(a) Chamber fully extended

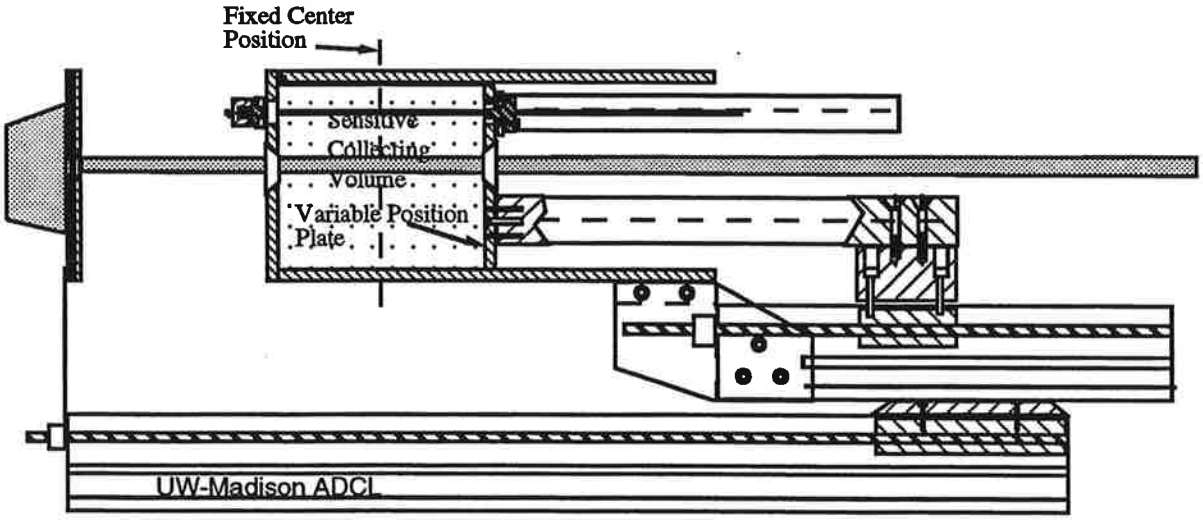

(b) Chamber not extended

Figure 4.2: The UW variable-length free-air ionization chamber is schematically illustrated. Note that the change in ionization current results from charge collected in the additional air volume created at the center of the chamber as it is extended.

same cross section and intensity as the beam at the aperture exit. A correction must be applied for the attenuation of the photon fluence between the diaphragm and the center of the chamber where the ionization is collected. Correction factors must also be applied for the gain of ionization from electrons generated by the photons scattered within the air of the chamber, which are not included in the definition of exposure, and for the ionization deficiency due to electrons that have not dissipated all of their energy in the air volume in the chamber.

The Attix free-air chamber is employed to make measurements with variable plate spacing about a fixed central plane. First an ionization measurement is made with the plate separation set at its maximum. Current is measured on the electrometer coulomb scale over a timed exposure. The chamber volume (plate separation) is then decreased by ΔL, ensuring the chamber central plane and defining aperture remain in fixed positions in space. This is accomplished by stepping slide assembly 1 one half the distance of slide assembly 2 and in the opposite direction (see Figure 4.2). The increase in charge collected is due to electrons originating in the incremental increase in volume in the center of the chamber as shown in Figure 4.2. The electrons deposit all of their energy in the chamber volume, except for those that strike the collecting rod, and produce the ionization measured. By determining the difference in charge collected for two plate separations, the effect of the unknown electric field lines near the chamber ends cancels so that the difference in charge is collected in a precisely known volume.

The exposure rate at the entrance aperture of a free-air chamber can be calculated from

$$\dot{X} = \frac{\Delta I}{\rho A_o \Delta L} e^{\mu' x} (1 - f_s + f_e) \qquad (1)$$

where ΔI is the ionization current, corrected to standard temperature and pressure,

ΔL is the plate separation [m],

ρ is the air density in [kg/m^3] at standard temperature and pressure,

μ is the linear attenuation coefficient [m^{-1}] for the appropriate photon energy in air,

A_o is the aperture area in [m^2],

x' is the distance from the aperture to fixed central plane of chamber,

f_s is the fraction of current produced by scattered electrons and Bremsstrahlung radiation, and

f_e is the fraction of current lost due to electrons striking the collecting rod or chamber walls.

For the UW free-air chamber, the ratio of ΔI to ΔL is actually the change in ionization current, ΔI, for a known change in plate separation ΔL. Charge collected over a fixed time interval may also be used for exposure calculations.

The air attenuation is experimentally measured to enable the exposure rate at the aperture to be calculated. The center of the collecting volume of the FAC is placed at the position the aperture is when exposure measurements were made. This permitted the measurement of the air attenuation over the same air space that the correction is applied over. The FAC plate separation was set to 100 mm. The chamber to aperture distance is varied, but the entire beam is completely contained by the chamber over the distances employed. Therefore, the observed changes in FAC reading can be attributed solely to photon attenuation in air. Table 3.3 shows the average linear attenuation coefficient as measured with the FAC compared with values determined from the spectral measurements.

4.4 UW-FAC Characterization

The UW-FAC was characterized with respect to saturation, minimum plate separation used during chamber operation and various aperture dependencies. The ionization saturation as a function of applied collecting potential for the Attix free-air chamber was measured on the UW-ADCL x-ray beam UW 50-M at an exposure rate of 165 mR/sec. The charge versus 1/voltage for the FAC is plotted in Figure 4.3 and extrapolated to the (1/voltage) = 0 axis to obtain the ionization for complete saturation. The data shows that an applied voltage of 2.5 kV is necessary to ensure minimum recombination of less than 0.2% in the chamber.

The correction for unwanted contribution of x-rays scattered out of the air column within the chamber was initially approximated with experimental data from Ritz [7]. The photon scatter correction factor accounts for the fact that the free-air chamber collects all the charge deposited from photon interactions inside its collecting volume. Fulfilling the definition of exposure requires collection of only the charge deposited in interactions occurring in the aperture defined volume, not from photons which scatter out of that volume and then interact. An experimental measure of this scatter effect as described in 1954 by Attix and DeLaVergne[8] would be difficult, if not impossible, due to the lack of axial symmetry in the chamber design. Therefore, monte carlo calculations were performed to determine this correction as described in Appendix A. Since the range for photons is considerably larger than the diameter of the chamber, a simple fluence calculation would over estimate this correction. Therefore, energy deposited per unit mass was calculated for the primary and scatter regions and then the ratio was multiplied by the ratio of masses of the primary and scatter regions to arrive at the correction factor. Details of the geometry and results of these calculations are given in the appendix.

To determine the range of plate separations to be used, a series of measurements was made on the UW 50-M and 20-M x-ray beams. The plate separation was set to its maximum

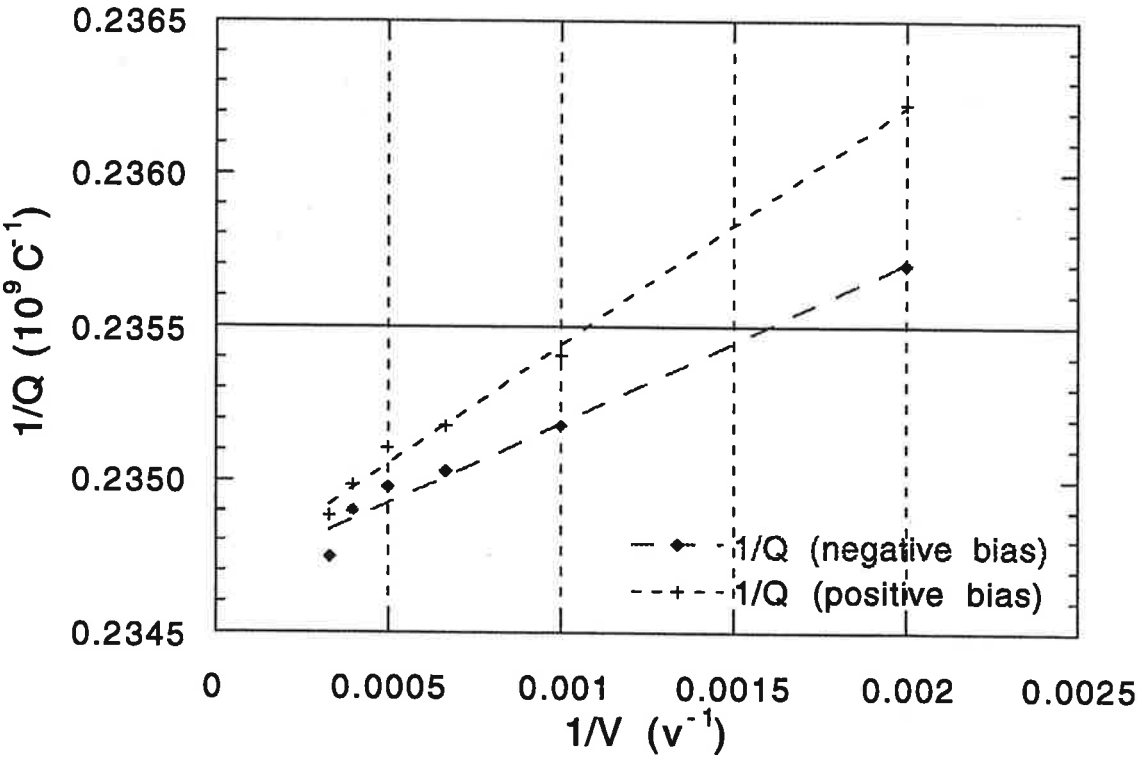

Figure 4.3: Saturation plot for UW free-air ionization chamber on UW-ADCL 50M tungsten anode aluminum filtered beam at an exposure rate of 165 mR/sec. Data are versus inverse voltage due to the moderately high LET of mammography energy photons.

of 200 mm and a measurement was made. The plate separation was decreased in 10 mm increments, moving the chamber backward 5 mm each time to maintain a stationary center of volume. The change in ionization current per change in plate separation is shown in Figure 4.4. Note that down to 40 mm nominal plate separation, the data are linear. At smaller plate separations, the signal drops off due to secondary electron non-equilibrium caused by insufficient build up and distortion of the electric field.

Two series of apertures with varying diameter and thickness were designed for the UW-FAC to investigate possible aperture scatter affects to the exposure measurements. Measurements were performed on NIST traceable orthovoltage beams at the UW-ADCL. No aperture related effects were observed for apertures with thickness of 5, 10 and 15 mm. Measurements made with the varying aperture diameters of 5, 7.5 and 10 mm showed exposure measurements increasing with increasing area. Effects of up to 2.4% were observed, depending on beam energy.

A series of measurements was made to investigate possible effect of exposure rate and source to free-air chamber distance on exposure measurements. Measurements were performed at focus to chamber distances of 0.50, 0.75, 1.0 and 1.5 m on the UW 20-M, 30-M, 40-M and 50-M orthovoltage beams. Exposure data at the 0.5 m distance were in disagreement by over 2% with the FAC data being lower than the ion chamber data. It was determined that due to the large focal spot size and 10 mm diameter aperture that the beam divergence was greater in diameter than the exit window of the FAC causing scatter of the primary beam and a loss of linearity of charge versus plate separation. Comparisons of measured exposure rates between the UW-FAC and the NIST calibrated PRM LE0.8 ionization chamber at all distances greater than 0.5 m showed disagreement between the two chambers of no greater than 0.4 % for all beams.

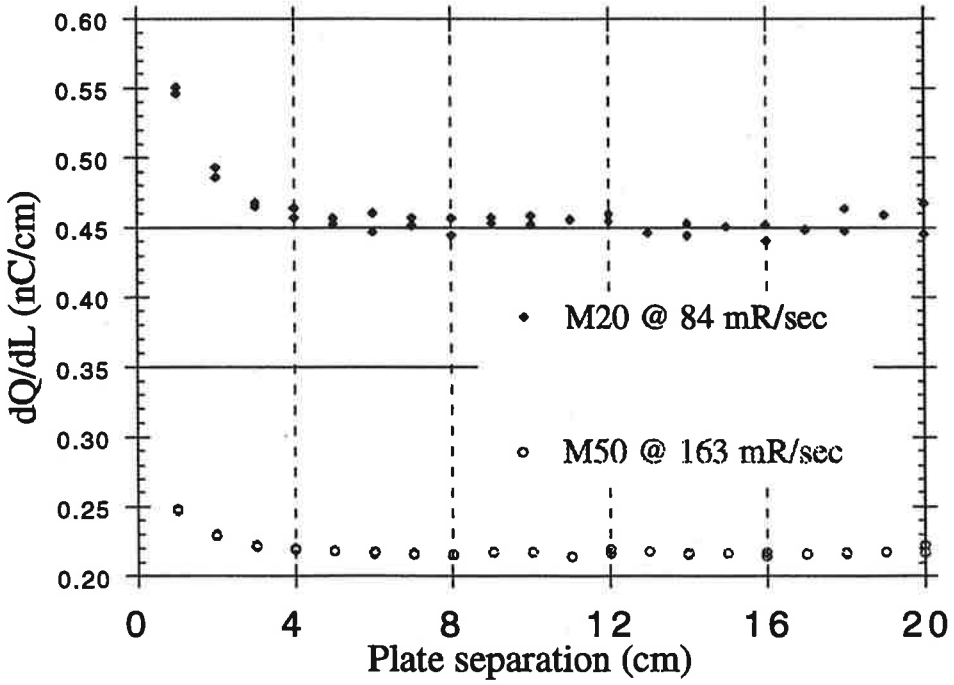

Figure 4.4: Change in ionization charge per plate separation versus plate separation for UW-ADCL tungsten anode aluminum filtered beams.

4.5 Uncertainty Assessment

The method of uncertainty assessment followed the recommendation of the Comite´ International des Poids et Mesures (CIPM). The uncertainty estimates are of two kinds: Type A are random uncertainties derived as standard deviations of the mean of quantities that are repeatedly measured. Type B are subjective best estimates of uncertainties based on the extensive experience of the calibration staff and are estimated to correspond to approximately a 67% confidence limit. Type A can be thought of as the precision of the measurement while type B represents the accuracy. Type A and B uncertainties are combined by taking the quadratic sum of each type separately and then are combined by the same quadratic method to obtain the one standard deviation (1σ) percentage uncertainty for A and B types together. This is doubled to yield the overall uncertainty of the measurement, that is its percentage uncertainty at the two standard deviation (2σ) or 95% confidence level.

For the UW-FAC, this uncertainty assessment was performed for each of the parameters affecting the quantities of equation 1; a discussion of these parameters follows. For charge, Type A is the average coefficient of variation for charge measurments made with the FAC. Type B includes the accuracy to which a coulomb of charge can be measured with a calibrated electrometer. The various diameters of the aperture were measured under magnification to an accuracy of better than 25 μm. The pitch of the screw drive controlling the plate separation is 1mm and is driven by a stepping motor with 400 steps per revolution. The uncertainty associated with the ability to return to the same plate separation is reflected in the precision of the first and last charge measurements which are made at the same plate separation for each beam. The uncertainty in humidity refers to the uncertainty in correcting charge measurements to dry air conditions. Since the free-air chamber has a large volume, it is more sensitive to ambient radiation background than the much smaller volume field instruments. The uncertainty in electric field distortion accounts for possible variation of the

Table 4.1: Uncertainties in determination of exposure rate from variable-length free-air chamber measurements.

Quantity	Type A	Type B
Aperture area	0.01 %	0.03 %
Change in plate separation, ΔL	0.07	0.01
Charge	0.10	0.10
Time	0.05	0.05
Air density	0.1	0.09
Recombination loss	0.1	N/A
Humidity	N/A	0.1
Leakage	0.1	N/A
Radiation background	N/A	0.01
Air attenuation	0.05	0.03
Photon scatter	N/A	0.05
Electron loss	N/A	0.01
Electric field distortion	N/A	N/A
Polarity difference	0.04	N/A
Aperture alignment	N/A	0.05
Penetration of chamber by scattered x-rays	N/A	0.04
Quadratic Sum	**0.227**	**0.198**
Combined Uncertainty	**0.30**	
Overall Uncertainty	**0.60**	

electric field as the chamber length is varied. The aperture alignment uncertainty estimates the ability to position the axis of the aperture parallel and coincident with the x-ray beam axis. This analysis, details of which are shown in Table 4.1, yielded an overall uncertainty for exposure measurements of 0.60% at the 95% confidence level for the UW variable-length free-air ionization chamber.

4.6 Free-Air Chamber Comparison

The direct comparison with the National Institute of Standards and Technology low-energy exposure standard was made to ensure the accuracy of the UW chamber on NIST standard tungsten anode aluminum filtered x-ray beams. The UW-FAC could then be used in confidence on other low energy photon beams as an exposure standard.

The two free-air chambers were designed for different ranges of the x-ray spectrum and therefore a meaningful comparison can only be made over energies common to both chambers. The x-ray system employed during this intercomparison consisted of a tungsten anode tube with approximately 1.0 mm of beryllium filtration and a constant potential generator. The tube voltage and current were continuously monitored. The tungsten generated aluminum filtered NIST x-ray beam codes used for this intercomparison are listed along with beam characteristics in Table 4.2.

Corrections for scattered photon contribution were calculated from data from Ritz [6]. Air attenuation correction factors to account for air attenuation between the aperture and center of the chamber were measured previously for the air path length of 127 mm for the Ritz chamber. Air attenuation corrections were experimentally determined for the air path-length of 169 mm for the UW FAC on the day of comparison. The correction factors for the Ritz and UW FACs employed for exposure calculation are shown in Table 4.3.

TABLE 4.2: Half-value layers (HVL) in mm of aluminum and homogeneity coefficients (HC) for NIST low-energy x-ray beams used in the exposure standard comparisons.

NIST beam	HVL (mm Al)	HC (%)
M20	0.152	79
M30	0.36	64
M40	0.73	66
M50	1.02	66
L20	0.071	76
L30	0.22	60

The Ritz and UW chambers were positioned on a support system perpendicular to the beam axis which enabled either chamber to be brought into the x-ray beam. A HeNe laser along the axis of the beam was used to align the axis of the free-air chambers. A telescopic positioning device on the edge of the cart system permitted the accurate alignment of the defining plane of each aperture at the same distance from the x-ray source. A 12.7 mm aperture positioned in front of the x-ray tube limited the beam size at 500 mm to a uniform field slightly larger than the FACs' apertures.

A thin-window parallel-plate transmission monitor was used to normalize the response of the free-air ionization chambers to variations in the x-ray tube output. The same electrometer was employed to measure the currents for both FACs. Leakage measurements were taken prior to and after each irradiation and then subtracted from the ionization currents. Average leakage for the UW FAC was -1.29×10^{-13} A (0.02% of signal) and for the Ritz FAC was -3.48×10^{-14} A (0.003% of signal).

The results of this chamber comparison are given in Table 4.4. The exposure rates measured by each FAC were at different times, therefore the percentage difference data are normalized to the transmission monitor current collected with each set of data. The results indicate that direct comparison exposure measurements with two FACs, with quite different geometries, can be made in the low-energy x-ray region with a discrepancy of less than 0.24%.

TABLE 4.3: Correction factors applied to Ritz and UW FACs for the NIST tungsten anode beams. Here, f_S is the fraction of current produced by scattered photons and Bremsstrahlung radiation, and f_e is the fraction of current lost due to electrons striking the collecting rod or chamber walls.

	Ritz			UW		
NIST	f_e	f_S	air attn.	f_e	f_S	air attn.
M20	0	0.006	1.0639	0	0.007	1.0867
M30	0	0.0053	1.0288	0	0.006	1.0391
M40	0	0.0048	1.0169	0	0.0055	1.0228
M50	0	0.0045	1.0113	0	0.005	1.0152
L20	0	0.0067	1.1327	0	0.0067	1.1759
L30	0	0.0058	1.0503	0	0.006	1.0667

TABLE 4.4: Comparison of UW FAC exposure rates and those determined by NIST Ritz 20-100 kVp FAC. The percentage differences are based on data normalized to transmission monitor currents.

NIST beam code	UW FAC [R/sec]	Ritz [R/sec]	% diff.
M20	0.3540	0.3557	-0.24
M30	0.3156	0.3160	-0.24
M40	0.3249	0.3252	-0.04
M50	0.3666	0.3662	+0.16
L20	2.0626	2.0496	+0.03
L30	0.4924	0.4929	+0.22

4.7 Conclusions

A free-air ionization chamber permits the direct and absolute measure of exposure in low-energy x-ray beams. An Attix style free-air ionization chamber was designed and constructed for ionization chamber calibrations at mammography energies. A direct comparison of this Attix-style free-air chamber with the NIST 20-100 kV free-air chamber was performed to ensure the accuracy of the Attix chamber on NIST standard tungsten-anode aluminum-filtered x-ray beams. Comparisons were made on the NIST M-20, M-30, M-40 and M-50 moderately filtered and the L-30 and L-40 lightly filtered x-ray beams. NIST has assessed the overall uncertainty associated with the measurement of the exposure rate of an x-ray beam with a parallel plate FAC to be 0.7% [9] while we have determined the uncertainty to be 0.54% for the Attix-style FAC. Disagreement between the NIST 20-100 kV and UW free-air chambers is less than 0.24%, well within the uncertainty expected for such an intercomparison.

4.8 References

[1] F. H. Attix, *Introduction to Radiological Physics and Radiation Dosimetry*, John Wiley and Sons, New York (1986).

[2] F. H. Attix, "Electronic Equilibrium in Free-Air Chambers and a Proposed New Chamber Design," Naval Res. Lab. Rep. No. 5646 (1961).

[3] R.F. Laitano and M. P. Toni, "The primary exposure standard of ENEA for medium energy x-rays. Characteristics and measurement procedures." Report RT/PROT (83) 27, Laboratorio di Metrologia della Radiazioni Ionizzani ENEA, CRE Casaccia, c.p. 2400 Roma, Italia (1984).

[4] C. M. Meger, "Dosimetry and Radiobiology of Synchrotron Produced Ultrasoft X-rays," Ph.D. thesis, UW-Madison (1989).

[5] J. G. Coletti, D. W. Pearson, and L. A. DeWerd, "Mammography Exposure Standard: Design and Characterization of Free-Air Ionization Chamber," Rev. Sci. Instrum. **66**(3), 2574-2577 (1995).

[6] V. H. Ritz, "Standard Free-Air Chamber for the Measurement of Low-energy X-rays (20 to 100 Kilovolts-Constant-Potential)," Journal of Res. of the Nat. Bur. of Standards, **64C**, 49-53 (1960).

[7] V. H. Ritz, "Design of Free-Air Ionization Chambers for the Soft X-Ray Region 920-100 kV)," Radiology, **73**, 911-922 (1959).

[8] F. H. Attix and L. DeLaVergne, "Plate-Separation Requirements for Standard Free-Air Ionization Chambers," Journal of Res. of the Nat. Bur. of Standards, **53**, 393-402 (1954).

[9] P. J. Lamperti, T. P. Loftus, and R. Loevinger, "Calibration of X-Ray and Gamma-Ray Measuring Instruments," NBS Special Publication 250-16 (1988).

CHAPTER 5 IONIZATION CHAMBER CALIBRATIONS

5.1 Field Instruments

The ionization chamber is the most widely used type of dosimeter for precise exposure measurements. Cavity ionization chambers come in many varieties, but most basically consist of a solid envelope surrounding an air-filled cavity in which an electric field is established to collect the ions formed by radiation. Cavity chambers offer many advantages over free-air chambers including compactness and multidirectionality. Spherical or cylindrical chambers having gas volumes of 0.1 - 3 cm^3 are the most common forms of cavity ion chambers, but flat cavity chambers, generally referred to as parallel plate chambers, have an advantage for low energy photon applications. Parallel plate chambers can be constructed with thin foils of plastic membranes for one or both of the flat walls, causing only minimal attenuation or scattering of the incident soft energy x-rays.

For exposure measurements in fields of photons under charged-particle equilibrium, chamber walls should be thick enough to (a) keep out of the cavity any charged particles that originate outside of the wall and (b) provide at the cavity an equilibrium charged-particle fluence and spectrum that is fully characteristic of the photon interactions taking place in the wall material. For photon fields, the required wall thickness can conservatively be taken as being equal to the range of the maximum-energy secondary electrons set in motion by the photons in the wall itself.

Air is of special interest as a wall material for photon dosimetry because of its role as the reference medium for the definition of exposure and its convenience as an ion chamber gas. "Air-equivalent" chamber walls are often used. Air equivalency requires the matching of its mean mass energy-absorption coefficient to that of air for the photon spectrum present and the matching of the mean mass collision stopping powers for the

Table 5.1 Identification, volume and window construction for ionization chambers calibrated in this study.

Company	Model	Serial Number	Volume [cm^3]	window construction
MDH	10X5-6M	78900	6	0.7 mg/cm^2 metalized polyester
MDH	10X5-6	13497	6	0.033 mm polycarbonate thimble + 0.031 mm polycarbonate electrode
CNMC	303	1018037	3	30 mg/cm^2 polycarbonate
CNMC	315	826014	15	30 mg/cm^2 polycarbonate
PTW	N23344	669	0.2	2.5 mg/cm^2
Capintec	PS-033	CII.338499	0.5	0.5 mg/cm^2 PET - aluminum
PRM	LE0.8	8835	0.8	0.127 mm beryllium
PRM	TLE-2	3001	2.0	0.125 mm beryllium + 0.125 mm beryllium collector
PRM	MC-1	8808	1.0	0.25 mm beryllium
Exradin	A-3	154	3.6	0.25 mm C552 (air eq. material)
Keithley	96035	18691	15	32 mg/cm^2 graphite coated acrylic
Exradin	A11-TW	103	0.6	0.004 g/cm^2 C552 (air eq. material)
Standard Imaging	MAGNA	M950121	1.0	0.025 mm Kapton/graphite
Keithley	96035b	57337	15	diag - 32 mg/cm^2 graphite coated acrylic + 0.025 mm aluminum mammo - 32 mg/cm^2 graphite coated acrylic

secondary-electron spectrum present. These conditions in general can not be satisfied simultaneously. In mammography energies where the photoelectric effect is dominant, its Z-dependence is so much stronger than that of the stopping power that the second matching requirement is disregarded.

In this study, a representative sampling of ionization chambers currently used in mammography exposure and half-value layer measurements were calibrated against the Attix free-air ionization chamber. The physical characteristics of these chambers are presented in Table 5.1.

5.2 Calibration Protocol

The procedure followed to calibrate the response of an ionization chamber is the substitution technique as used in the UW-ADCL calibration protocol. The exposure rate at a point on the beam axis, either at 50 cm or 100 cm, is determined from free-air chamber measurement as explained in Chapter 2. The FAC is removed and the field instrument is placed with its calibration point at the same point on the beam axis as the exit of the FAC aperture. For most chambers, the calibration point is the center of the chambers collecting volume. If the chamber's center is not identifiable, the calibration point is chosen to be either the front window or the inner proximal surface. Bias voltage of +300 volts is applied to the chamber to be calibrated and it is allowed to equilibrate for about 15 minutes in the radiation field. The chamber is then exposed to the calibrated beam for period of time equal to that which the FAC was exposed. The response of the chamber is normalized to the transmission monitor response. Readings are collected until a set of four pairs is obtained for which the ratios of the chamber to be calibrated and the monitor chamber readings exhibit no monotonic change with sequential exposures. The four readings should have a standard deviation of less than 0.20% of the sample mean. A calibration factor, N_x, is assigned to the chamber by dividing the calibrated beam exposure rate by the field instrument response per

transmission monitor normalized to standard temperature and pressure and electrometer range calibration factor, as shown in the following equation:

$$N_X = \frac{\left(X_{FAC} / Q_{mon,FAC}\right)}{\left(Q_x / Q_{mon,x}\right)} \qquad (1)$$

where X_{FAC} is the exposure measured with the free-air chamber,

$Q_{mon,FAC}$ is the average charge reading of the monitor chamber during FAC irradiation,

Q_x is the average charge reading for the chamber to be calibrated,

$Q_{mon,x}$ is the average charge reading of the monitor chamber during chamber irradiation.

All charge measurements are corrected for the electrometer calibration factor for the range used. The exposure calibration factor is reported in units of roentgens / coulomb (R/C), corrected to standard temperature and pressure. No correction for ionic recombination is made for field instrument calibrations. All instruments in this study were open to atmospheric communication.

The uncertainty associated with these N_X values is dependent on the uncertainty in exposure as measured with the UW-FAC plus the uncertainty from the charge measurements with the individual field instruments being calibrated. These uncertainties were determined following the method as given in Chapter 4 Section 5 and are detailed in Table 5.2. Since the same electrometer and timing circuitry were employed for the charge measurements made with both the free-air chamber and the field instruments and the calibration factor is determined as a ratio, the Type B uncertainties for these quantities are zero. The calibration factors reported are for calibrations performed at a source to chamber distance of 1 m, enabling the uncertainty in chamber position and field uniformity to be small. These calculations yield an overall uncertainty of 0.68 % at the 95% confidence level.

Table 5.2: Uncertainties in calibration of N_x factor for field instruments from variable-length free-air chamber exposure measurements.

Quantity	Type A	Type B
Charge	0.08 %	0.0 %
Time	0.05	0.0
Air density	0.1	0.1
Recombination loss	0.01	N/A
Distance from source	0.01	N/A
Beam uniformity	0.1	N/A
Quadratic Sum	**0.171**	**0.100**
Combined Uncertainty		**0.20**
UW-FAC Uncertainty		**0.30**
Quadratic Sum		**0.36**
Overall Uncertainty		**0.72**

5.3 Exposure rate data

The exposure rate for each beam in this study was measured on the day of chamber calibrations with the UW-FAC. The data shown in Tables 5.3 and 5.4 represent the average exposure rates including all of the data for each beam. The exposure rate data for the NIST tungsten anode beams are shown in Table 5.5 for comparison.

Table 5.3 Average exposure rate data measured with UW-FAC for UW-ADCL M- and L-series tungsten anode aluminum filtered beams.

Beam Code	kVp	mA	X-rate @ 100 cm (R/sec)
20-M	20	10	0.0687
30-M	30	10	0.0702
40-M	40	10	0.0678
50-M	50	10	0.0861
30-L	30	10	0.1128
40-L	40	10	0.1134
50-L	50	10	0.1275

Table 5.4 Average exposure rate data measured with UW-FAC for UW-ADCL molybdenum anode molybdenum filtered x-ray beams.

Beam Code	kVp	mA	Added filt. (mm Mo)	X-rate @ 100 cm (R/sec)
23		110	0.03	0.242
25		100	0.03	0.291
28		95	0.03	0.406
30		90	0.03	0.335
35		70	0.03	0.589

Table 5.5 Average exposure rates measured with NIST Ritz FAC for NIST M- and L-series tungsten anode aluminum filtered x-ray beams.

Beam Code	kVp	mA	Added filt. (mm Al)	X-rate @ 50 cm (R/sec)
M20	20	10	0.230	0.3557
M30	30	10	0.50	0.3160
M40	40	10	0.786	0.3252
M50	50	10	1.021	0.3662
L20	20	10	0	2.0496
L30	30	10	0.265	0.4929

5.4 Calibration Factors versus beam parameters

In this section calibration factors versus the half-value layer of the calibration beam for all ionization chambers in this study are presented. Each of the chambers was calibrated directly against an Attix free-air ionization chamber following the calibration procedure described previously in this chapter. Data are presented for beams from UW-ADCL constant potential tungsten anode with aluminum filtration and UW-ADCL clinical mammography molybdenum anode with molybdenum filtration. The beam parameters for these systems were described previously in Chapter 2 Section 4.

The experiences of calibration facilities have shown that ionization chamber calibration factors fall on smooth curves when plotted against the HVL of the calibration beam, provided that all calibration points have been chosen from a single beam series, L, M or H. If calibration points have been chosen from more than one series, discontinuities may occur due to the differences in the beam spectra occurring with changes in filtration.

The first set of data are for the PRM LE0.8 ionization chamber. This chamber is used by the UW-ADCL as its low energy transfer standard and therefore has a variety of NIST assigned calibration points. NIST assigns an overall uncertainty of 1% at the 95% confidence level to its x-ray calibrations. The factors assigned to this chamber on tungsten beams are consistent with the NIST assigned factors within the uncertainty associated with the calibration factor.

The second set of data are for the PRM TLE-2, a thin window transmission-type chamber designed specifically as a transfer standard. This chamber was provided by the Food and Drug Administration, Center for Devices and Radiological Health (CDRH) in Rockville, Maryland. The TLE-2 has calibration points on tungsten and molybdenum beams from the Physikalisch-Technische Bundesanstalt (PTB). Currently, the PTB is the only national standards laboratory providing exposure calibrations on mammography energy

molybdenum anode x-ray beams. NIST, CDRH and the ADCL at the UW-Madison are currently establishing molybdenum anode calibration ranges for mammography instrument calibration.

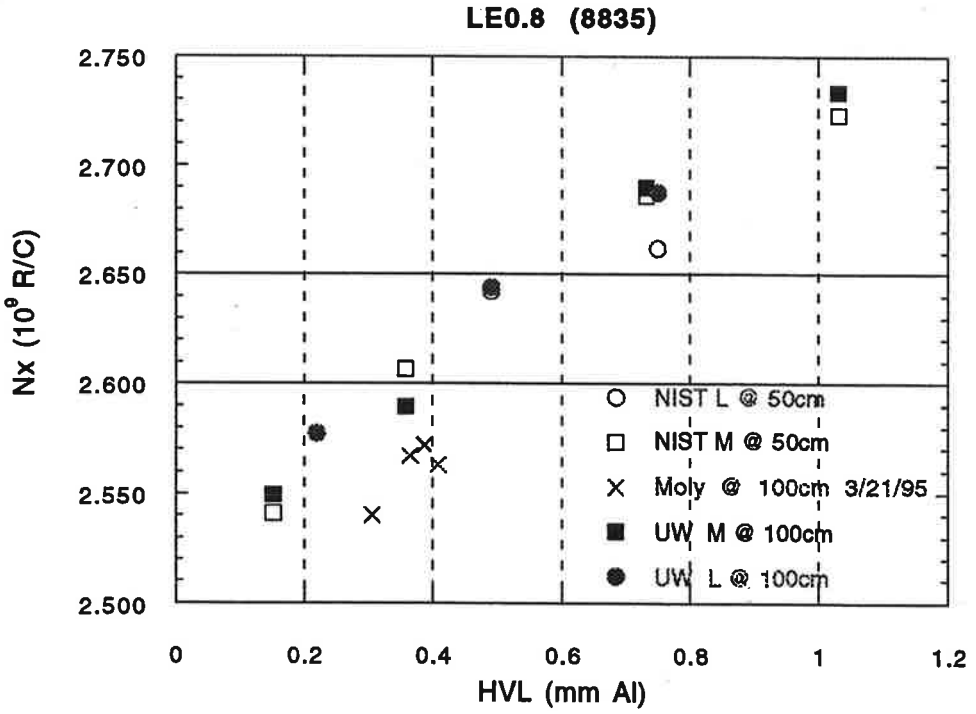

Figure 5.1 N_x values for PRM LE0.8 (8835) as assigned by UW-FAC on tungsten and molybdenum anode calibration beams.

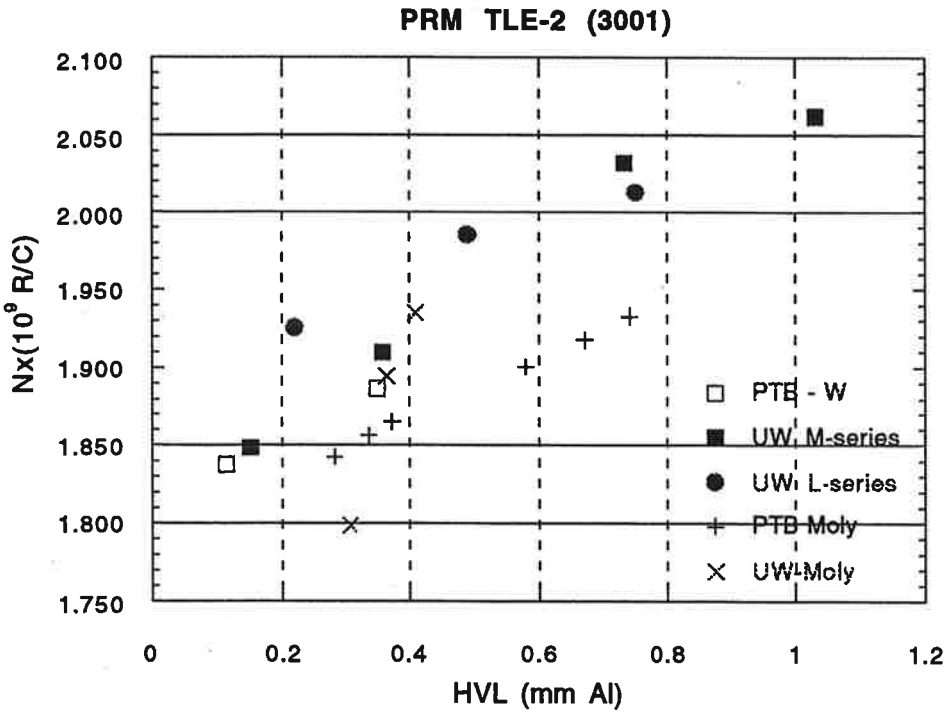

Figure 5.2 N_x values for PRM TLE-2 (3001) as assigned by UW-FAC on tungsten and molybdenum anode calibration beams.

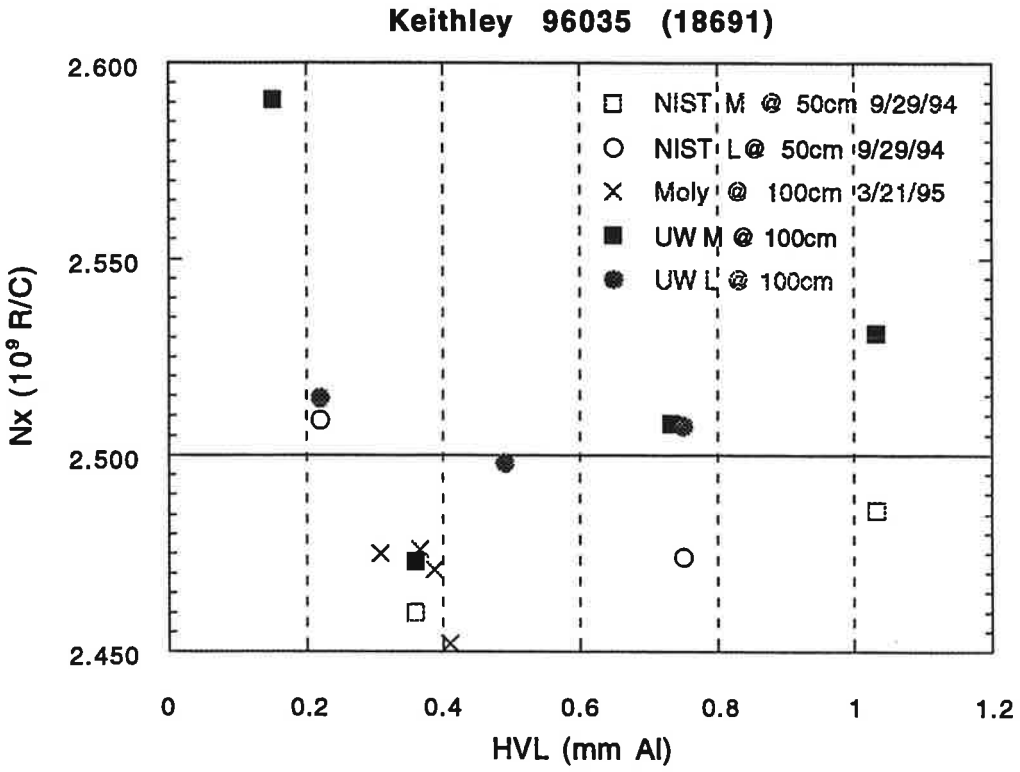

Figure 5.3 N_x values for Keithley 96035 (18691) as assigned by UW-FAC on tungsten and molybdenum calibration beams.

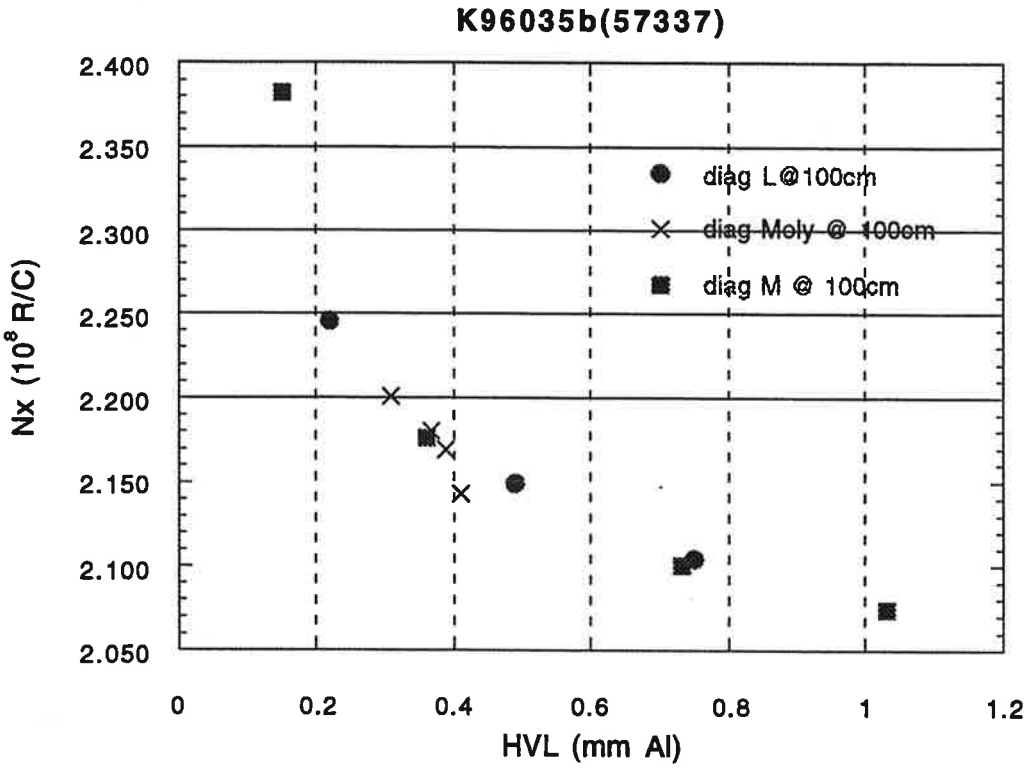

Figure 5.4 N_x values for Keithley 96035b, diagnostic (57337) as assigned by UW-FAC on tungsten and molybdenum anode calibration beams.

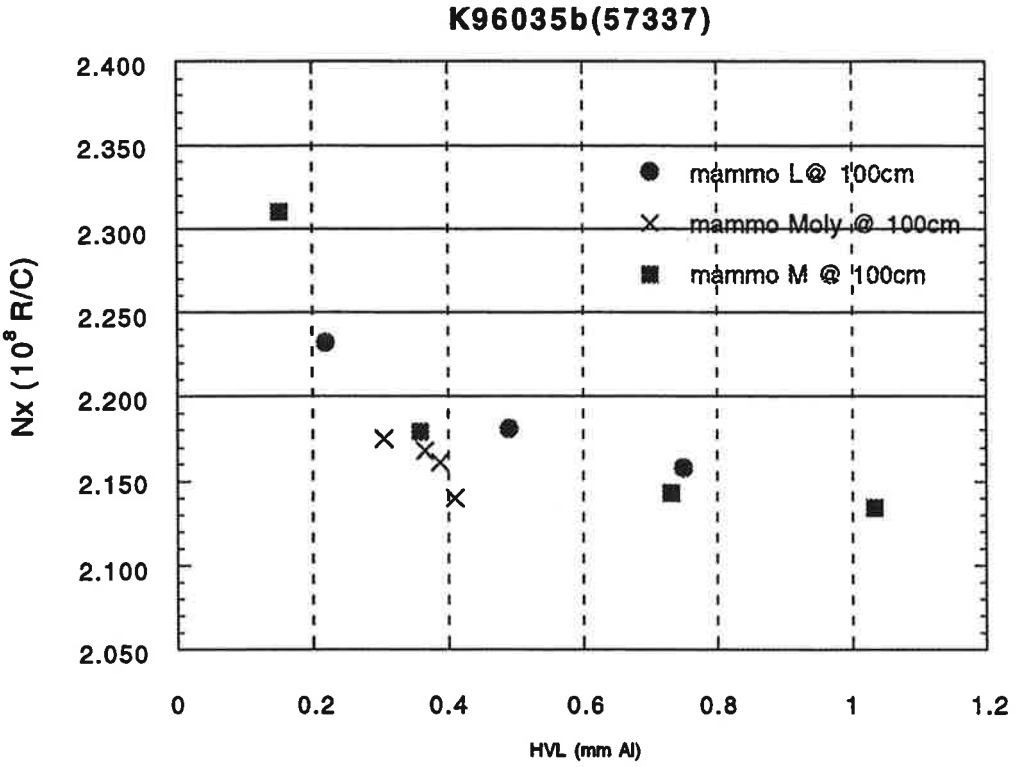

Figure 5.5 N_x values for Keithley 96035b mammographic (57337) as assigned by UW-FAC on tungsten and molybdenum anode calibration beams.

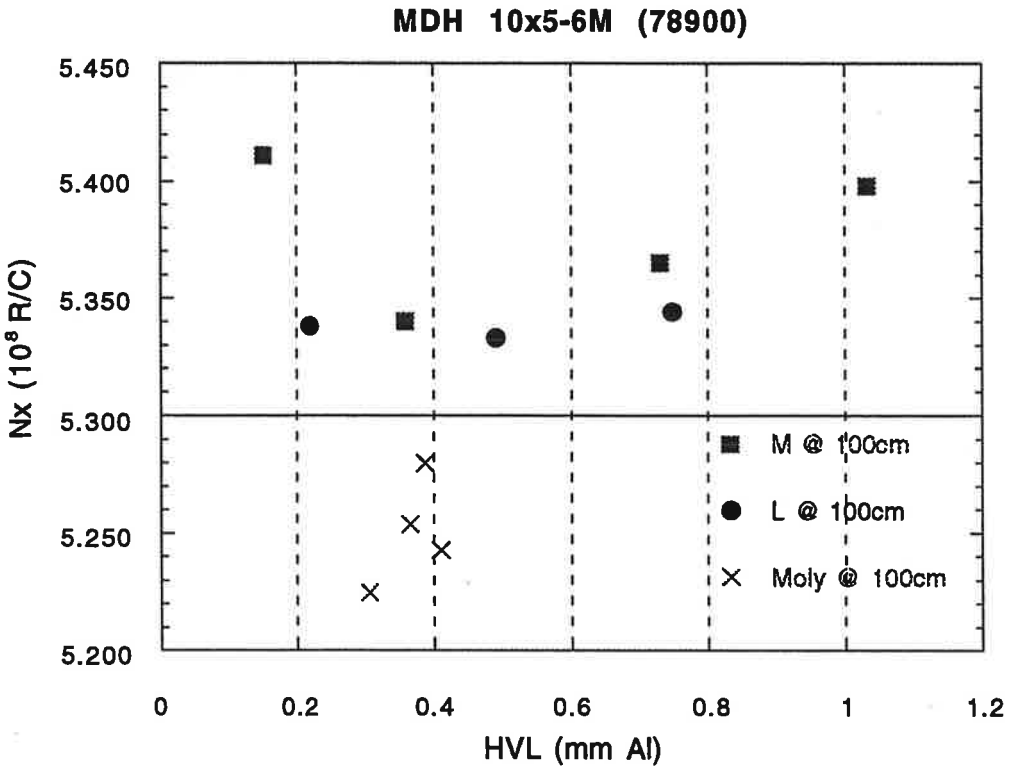

Figure 5.6 N_x values for MDH 10x5-6M (78900) as assigned by UW-FAC on tungsten and molybdenum anode calibration beams.

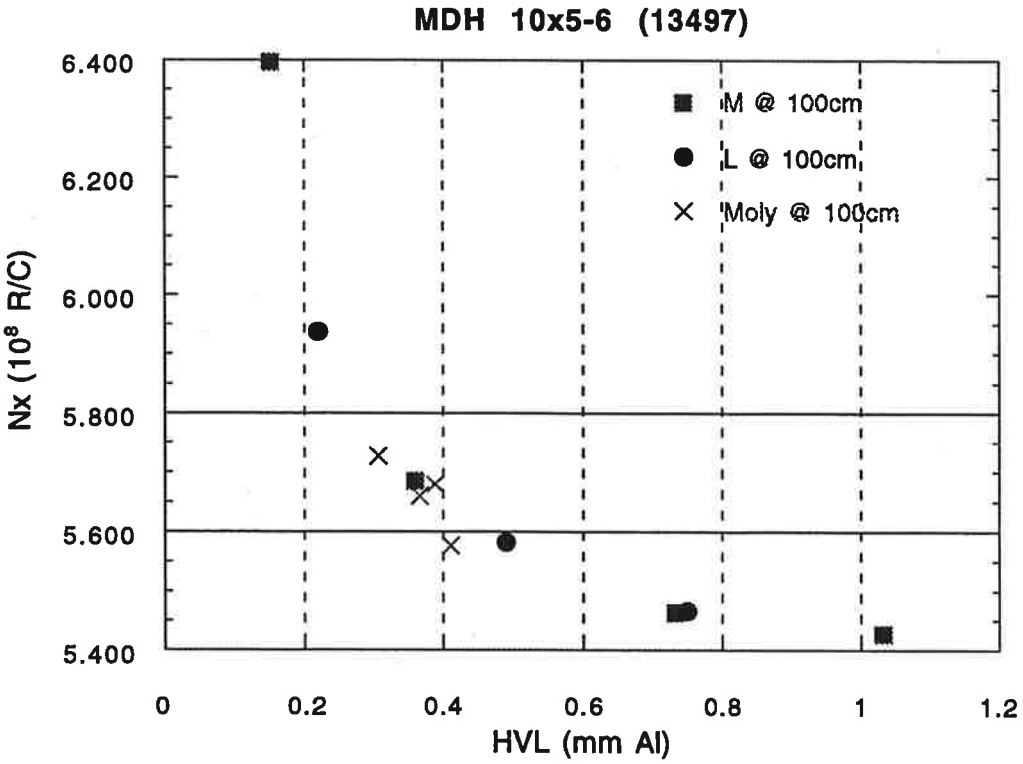

Figure 5.7 N_x values for MDH 10x5-6 (13497) as assigned by UW-FAC on tungsten and molybdenum anode calibration beams.

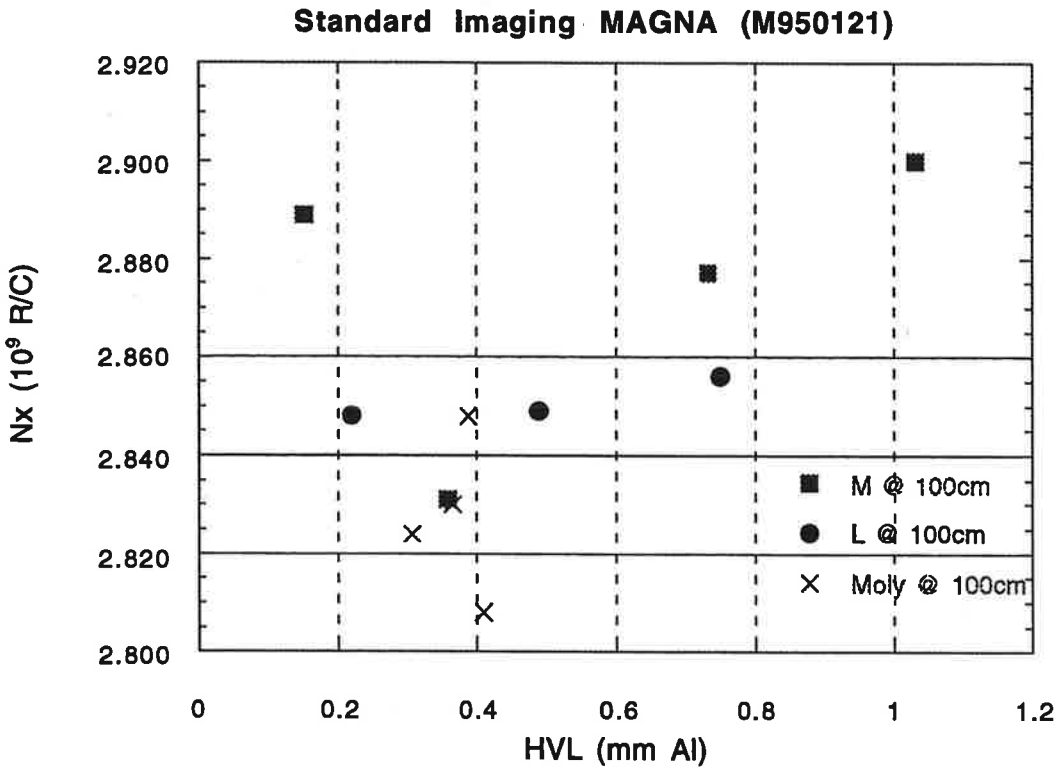

Figure 5.8 N_x values for Standard Imaging MAGNA (M950121) as assigned by UW-FAC on tungsten and molybdenum anode calibration beams.

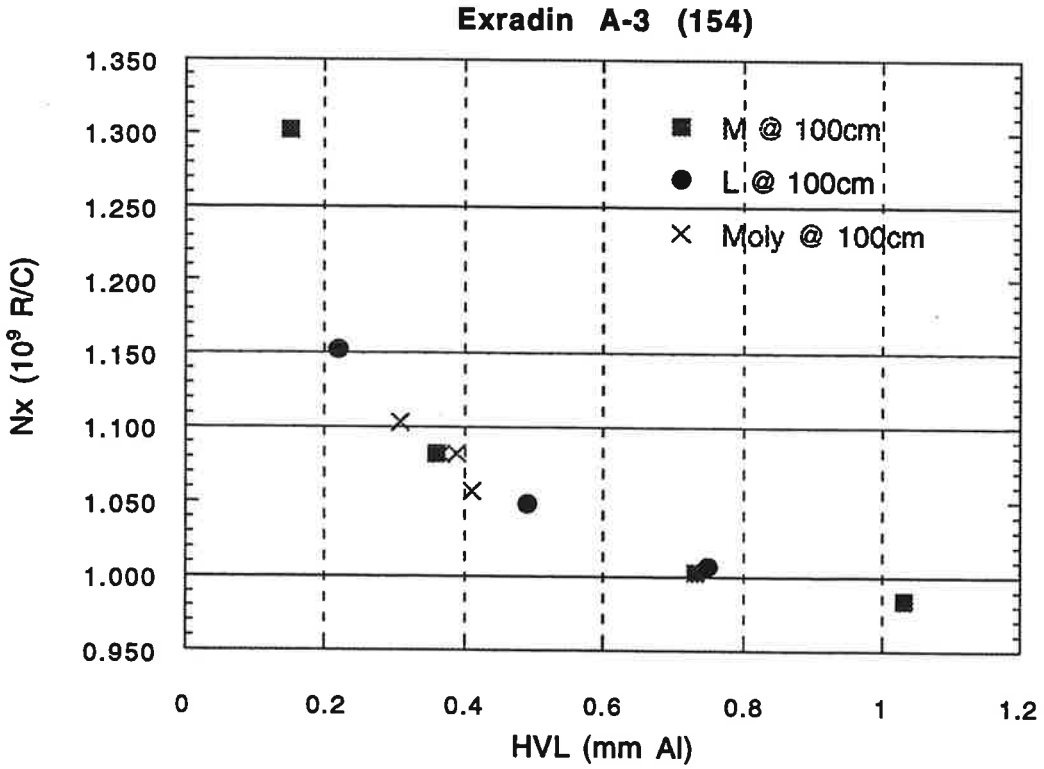

Figure 5.9 N_x values for Exradin A-3 (154) as assigned by UW-FAC on tungsten and molybdenum anode calibration beams.

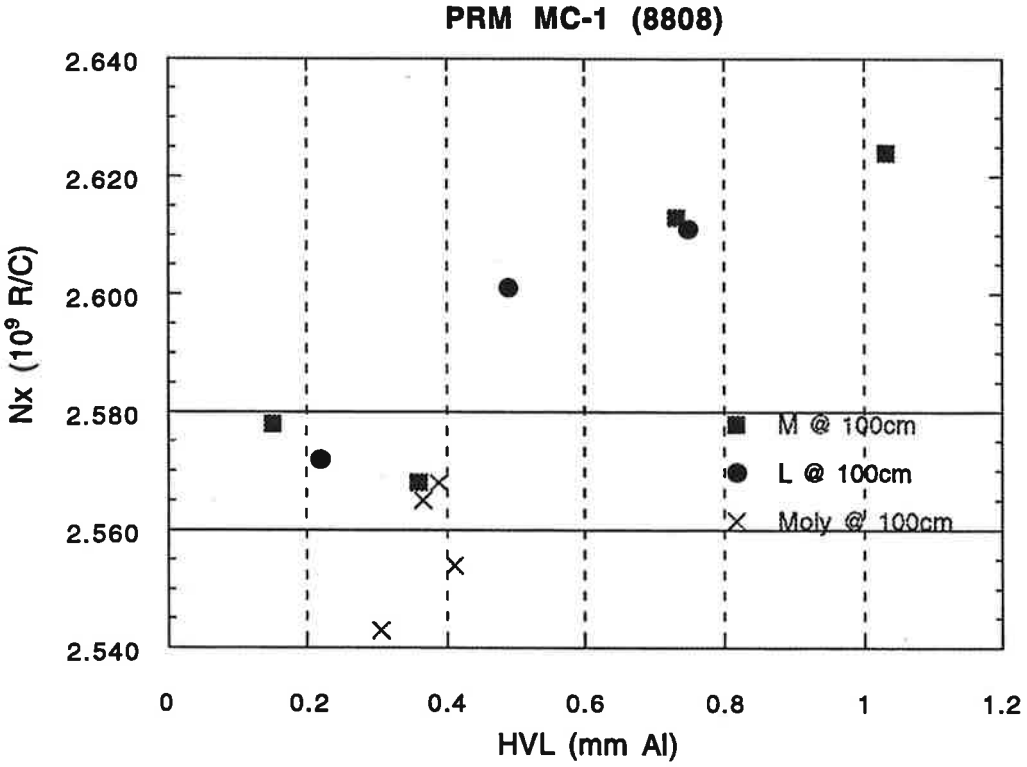

Figure 5.10 N_x values for PRM MC-1 (8808) as assigned by UW-FAC on tungsten and molybdenum anode calibration beams.

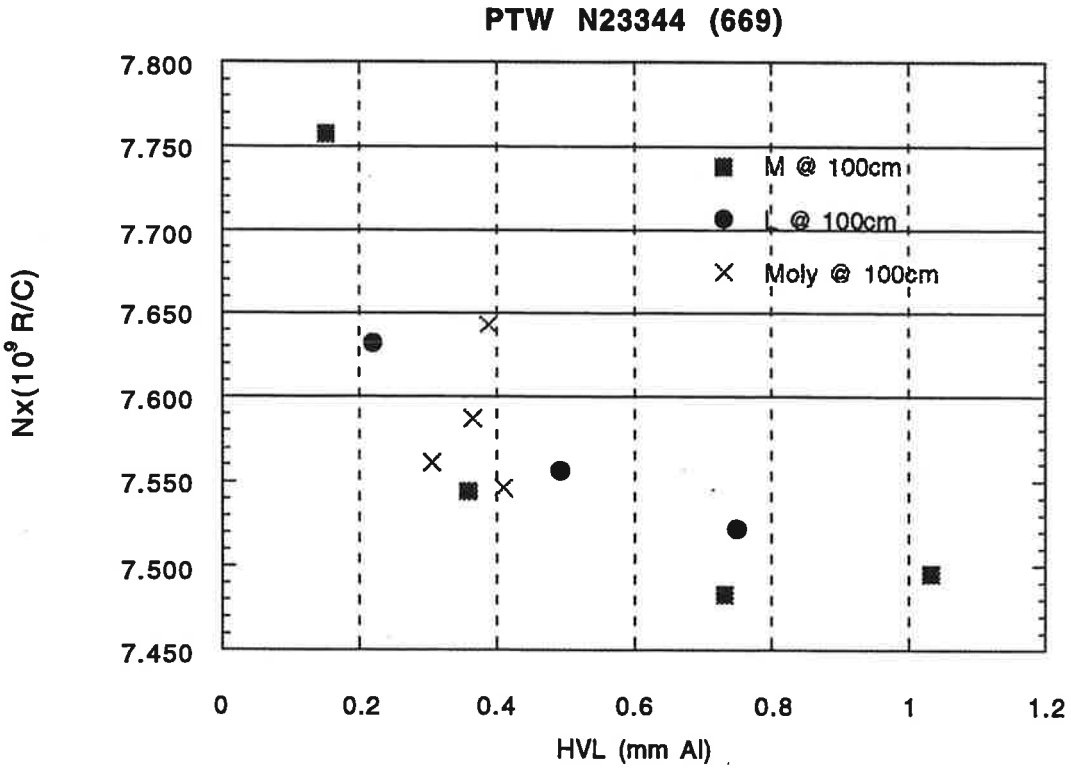

Figure 5.11 N_x values for PTW N23344 (669) as assigned by UW-FAC on tungsten and molybdenum anode calibration beams.

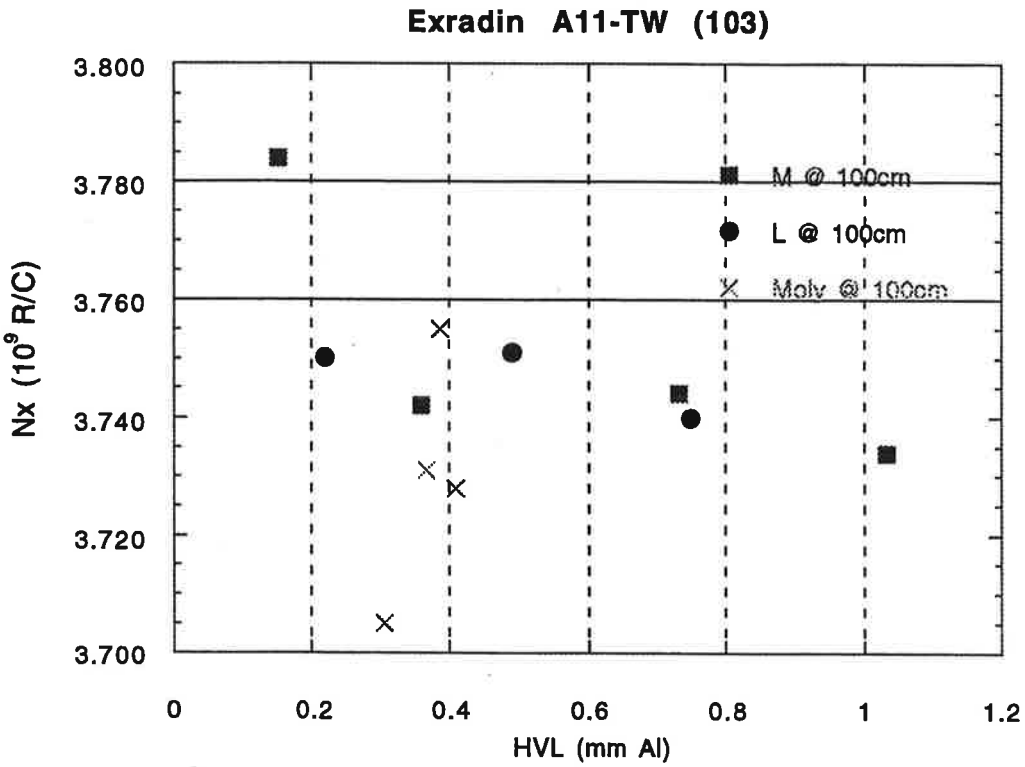

Figure 5.12 N_x values for Exradin A11-TW (103) as assigned by UW-FAC on tungsten and molybdenum anode calibration beams.

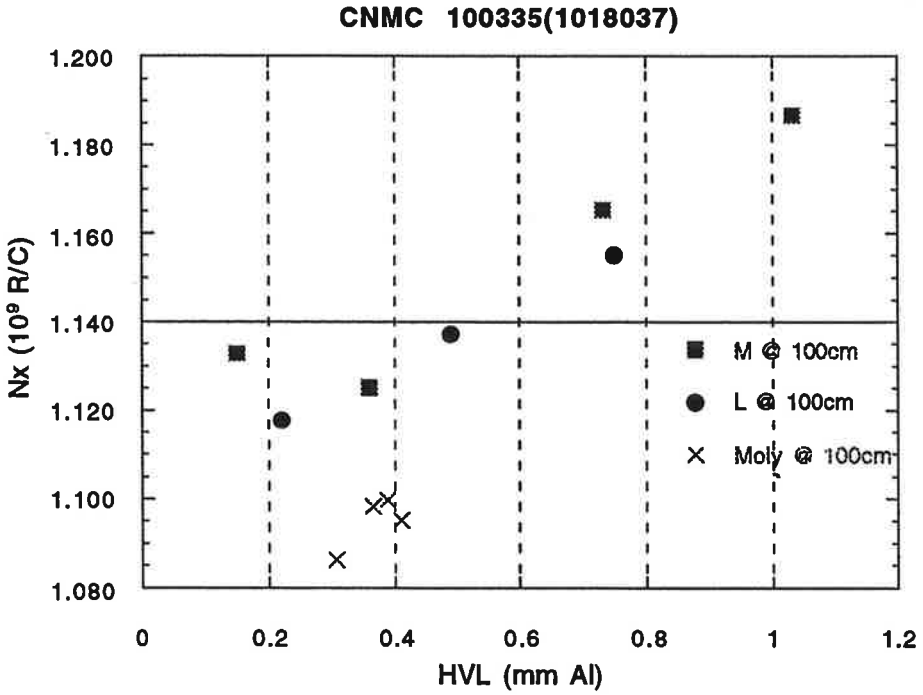

Figure 5.13 N_x values for CNMC 100335 (1018037) as assigned by UW-FAC on tungsten and molybdenum anode calibration beams.

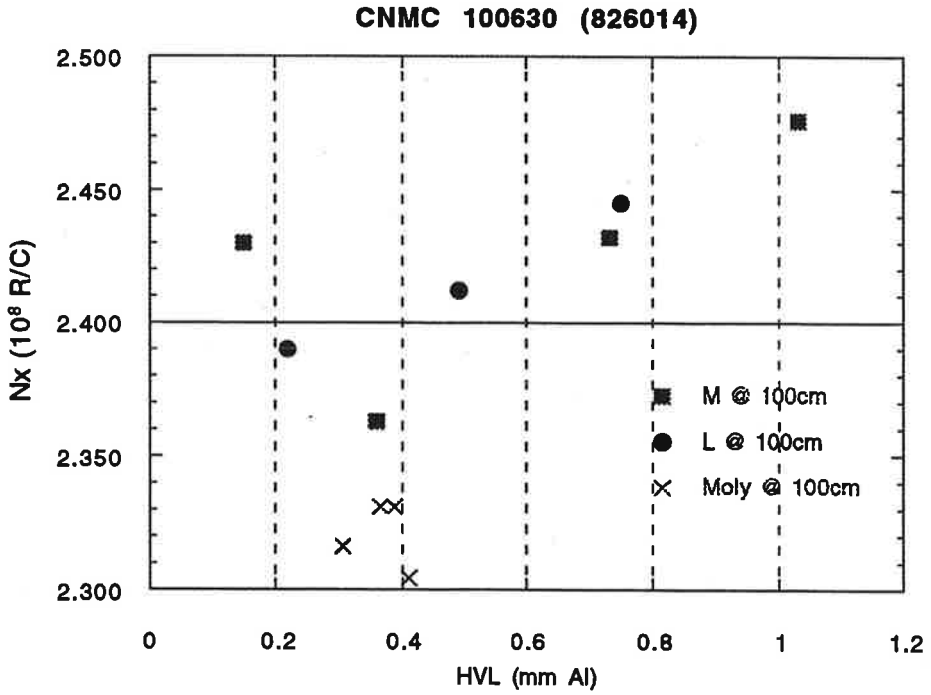

Figure 5.14 N_x values for CNMC 100630 (826014) as assigned by UW-FAC on tungsten and molybdenum anode calibration beams.

5.5 Discussion of ionization chamber calibration factors

The ionization chambers were calibrated against the UW-FAC following the protocol described in Section 5.2. The calibration factors for all chambers follow smooth curves when plotted against half-value layer for a specific series of beams. The data show that the calibration factors assigned to diagnostic ionization chambers in the mammography energy region display dependence on the half-value layer of the calibration beam. For most chambers, the molybdenum factors are about 2% lower than tungsten factors at the same HVL. Note that for chambers not specifically designed with thin entrance windows for the mammography energy region, the calibration factor increases significantly with decreasing HVL. The thicker chamber walls significantly attenuate the low energy photons, increasing the correction factor. These same chambers show little difference in response between tungsten and molybdenum beams of the same HVL. Field measurements of HVL made with such thick windowed chambers could be erroneous due to significant changes in chamber response with changes in beam spectra. This effect is discussed in the next section of this chapter. The PRM TLE-2 ionization chamber N_x values assigned on our high-frequency clinical molybdenum beams against the UW-FAC are consistent with the N_x values assigned to this chamber by the PTB on their constant-potential molybdenum calibration range. These data suggest that future calibration factors assigned to mammographic instruments on the constant-potential molybdenum-anode calibration beams currently being established will be accurate when the chambers are employed for exposure measurements on clinical high-frequency molybdenum beams.

5.6 HVL Dependence on Ion Chamber Energy Response

Half value layers for the tungsten M-series beams and the clinical molybdenum beams were measured with the UW-FAC as well as other ionization chambers which represent those with the greatest and least energy responses. These include the MDH 10x5-

6M, the PRM LE0.8 and the MDH 10x5-6. Figures 5.15 & 5.16 show plots of HVL measured with each of these chambers normalized to UW-FAC data versus kVp. Note that the FAC with its flat energy response yields the true values of HVL, since it accurately measures exposure as the spectrum changes due to the aluminum added to the beam. The LE0.8, which has an 8% variation in calibration factor over the range of mammography energies, displays a consistently low HVL. The MDH 10x5-6M, with its small variation in calibration factor of 2%, best agrees with the FAC measurements. The MDH 10x5-6 chamber has relatively thick walls for these low energy photon beams and has nearly a 20% energy dependence. The HVL determined with this chamber are consistently higher than the FAC measurements. To ensure the most accurate measurement of HVL, ionization chambers with the flatest energy response over the mammography energy region should be employed. This study shows a variety of ionization chambers that display variations in response of less than 5% over the range of mammography energies. Such a chamber should be employed for HVL measurements in mammography to minimize error introduced by changes in a chamber's response with changes in beam spectra.

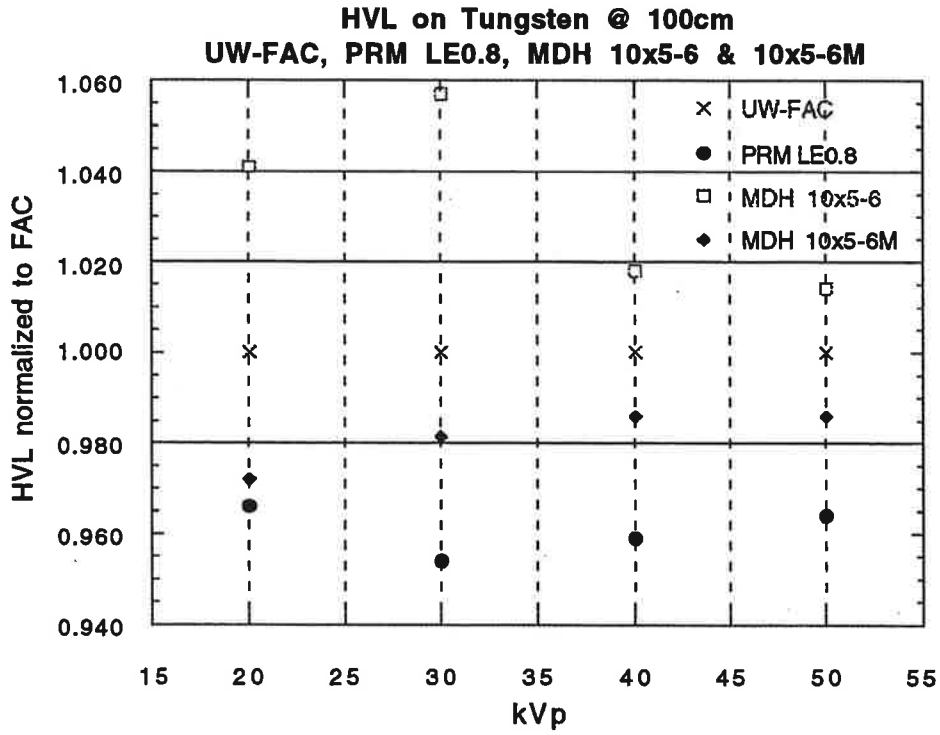

Figure 5.15 HVL for UW-ADCL tungsten anode beams measured with ionization chambers with differing energy responses. Data normalized to measurements made with UW-FAC.

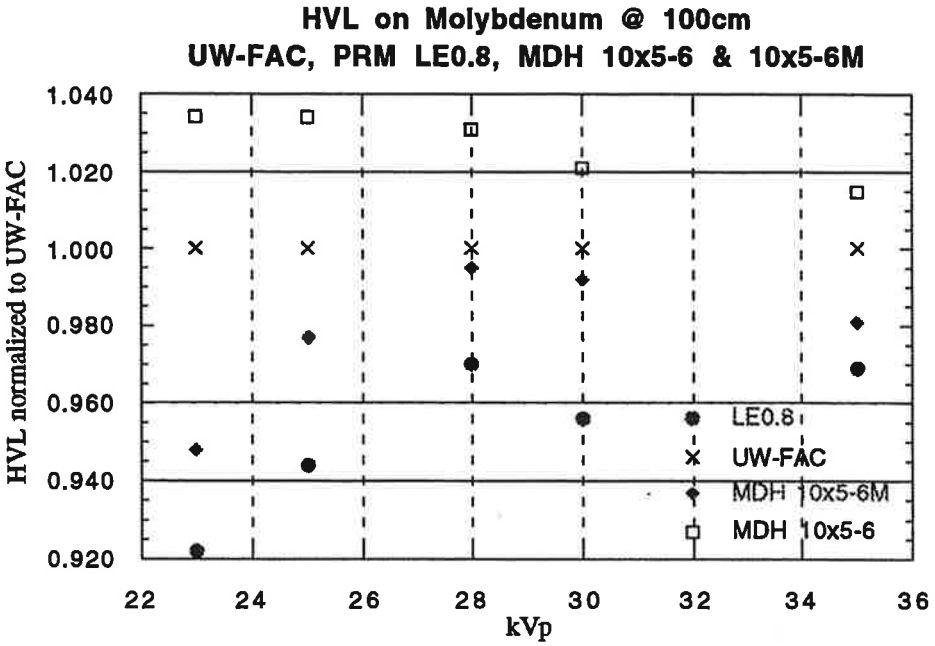

Figure 5.16 HVL for UW-ADCL molybdenum anode beams measured with ionization chambers with differing energy responses. Data normalized to measurements made with UW-FAC.

5.7 Effect on Mean Glandular Dose Calculations:

As described in Chapter 1 section 1, the mean glandular dose (MGD) is the preferred estimate of radiation risk associated with mammography. This dose is calculated by multiplication of the entrance skin exposure by a conversion factor which depends on beam HVL and breast thickness. An estimate of the error introduced to MGD calculations was made based on exposure and HVL measurements made with both a thin window ionization chamber and a thick window chamber designed for general diagnostic energies. The sample calculations were performed for a 25 kVp molybdenum beam and a 4.5 cm breast of 50% adipose / 50% glandular composition [1] and are shown in Table 5.6. As shown, these two factors could result in an error of up to 5.5% in the determination of MGD, in addition to those uncertainties already present due to uncertainty in breast thickness measurement, HVL and entrance skin exposure field measurement position, and uncertainty in the exposure to dose conversion factors themselves. Note that if calibration factors were assigned from molybdenum anode beams, the error in the determination of MGD would be reduced significantly.

Table 5.6 Calculation of error introduced into mean glandular dose measurement by ionization chamber energy response.

	UW-FAC	**Mammography chamber**	**Diagnostic chamber**
Error in ESE	0 %	-2.0%	+ 2.5 %
HVL	0.32 mm Al	0.30 mm Al	0.33 mm Al
Error in HVL	0 %	-2.2 %	+ 3.5 %
MGD / R	168 mRad / R	161.6 mRad / R	177.3 mRad / R
Error in MGD / R	0 %	- 3.8 %	+ 5.5 %

5.8 References:

[1] X. Wu, G.T. Barnes, D.M. Tucker, "Spectral dependence of glandular tissue dose in screen-film mammography," Radiology **179**: 143-148 (1991).

CHAPTER 6 CONCLUSIONS AND FUTURE INVESTIGATIONS

6.1 Conclusions:

This research attempted to quantify the accuracy of output exposure measurements of clinical mammography systems. Exposure measurements are currently made with ionization chambers which have been calibrated against the National Institute of Standards and Technology (NIST) traceable exposure standards in tungsten-anode constant-potential x-ray beams. Clinical mammography employs molybdenum-anode high-frequency x-ray systems. There are currently no NIST standard molybdenum-anode exposure standards. Therefore, a free-air ionization chamber based on a variable-length design by Attix [1] was constructed as an absolute exposure standard for mammographic energies. This chamber design was selected because measurements made at different plate separations permit the end effects of the electric field to be ignored and it permits air-attenuation measurements to be made with ease. The accuracy of this chamber was verified by direct comparison with the low-energy exposure standard maintained on tungsten-anode x-ray beams at the National Institute of Standards and Technology [2]. The disagreement between the NIST standard and the UW-FAC was less than 0.24% on mammography energy tungsten-anode x-ray beams.

The clinical molybdenum-anode and the calibration tungsten-anode x-ray beams were characterized with regard to kVp, first and second half-value-layers and photon energy spectra. A representative sample of ionization chambers currently used in diagnostic and mammographic quality assurance were calibrated against the variable-length free-air chamber in both the tungsten and molybdenum anode beams. The chambers designed for mammographic energies displayed a slightly higher response (~2%) per Roentgen in molybdenum anode beams than in tungsten anode beams of the same HVL. Thicker window chambers designed for higher energy diagnostic applications showed little

difference in response between the two spectra, but these chambers exhibit large changes in response with changes in beam energy. One chamber, the PRM TLE-2, had N_x values assigned from the PTB on constant-potential molybdenum anode calibration range. The N_x values assigned to this chamber against the UW-FAC on our high-frequency clinical molybdenum beams were consistent with the PTB values.

HVL measurements were made with a selection of these field instruments on both the tungsten and molybdenum beams. These measurements when compared to measurements made with the FAC showed variations of over 5% in HVL depending on the energy response of the chamber. To ensure the most accurate measure of HVL, chambers with the smallest energy response over the mammography energy range should be employed. A variety of thin-window chambers calibrated in this study displayed less than 5% energy response over the mammography energy range. Since the calculation of mean glandular dose depends on both the exposure calibration of the ionization and the HVL measurement, errors of 8% or more can be introduced to MGD calculations depending on the chamber used for the measurements of exposure and HVL.

6.2 Future Investigation:

At this time, calibration beams are being established with molybdenum and rhodium x-ray systems at NIST, the Center for Devices and Radiologic Health of the FDA and the ADCL at the University of Wisconsin - Madison. All three facilities have a variable-length free-air ionization chamber to use as an exposure standard for mammography energies. The comparison of the response of chambers between the clinical and calibration beams as well as variation in response between molybdenum and rhodium anode beams should be investigated to ensure continued accuracy in mammography exposure and HVL measurements.

APPENDIX A:

MONTE CARLO CALCULATIONS OF SCATTER PHOTON CORRECTION FACTOR:

The photon-scatter correction factor accounts for the fact that the free-air chamber collects all the charge deposited from photon interactions inside its collecting volume. Fulfilling the definition of exposure requires collection of only the charge deposited in interactions occurring in the aperture defined volume, not from photons which scatter out of that volume and then interact. Since the range for photons is considerably larger than the diameter of the chamber, a simple fluence calculation would over estimate this correction. Therefore, energy deposited per unit mass was calculated for the primary and scatter regions and then this ratio was multiplied by the ratio of masses of the primary beam and scatter regions to arrive at the appropriate correction factor.

The photon scatter correction factors for the free-air ionization measurements were determined by Monte Carlo calculations. Physical measurements of this correction were not possible due to the asymmetric geometry of the free-air chamber, in particular its off-center collecting rod. Ritz made physical measurements [1] on NIST's low-energy FAC using the method from Attix and DeLaVergne [2]. A tube of nearly air equivalent material extending the full length of the chamber enclosure is positioned inside the chamber, so that the x-ray beam passes through it from end to end. The tube must have walls thick enough to stop the electrons, but thin with respect to attenuation of scattered x-rays. To minimize field distortion, the tube could be coated with graphite and operated at half the chamber bias. The ratio of ionization measured with the tube in place to that with it removed will give the fraction of the total ionization that is contributed by scattered x-rays. The data taken from Ritz for a 5 cm diameter chamber are shown in Table A1.

kVp	scattered photon %
20	0.68
30	0.56
50	0.53

Table A1. Contribution of secondary photon ionization within FAC radius of 4.45 cm.

A.1 MCNP CODE:

The Monte Carlo code selected for this calculation was MCNP-4A, Monte Carlo N-Particle Transport Code System [3 & 4], part of the RSIC (Radiation Shielding Information Center) Computer Code Collection available through Oak Ridge National Laboratory. The code was developed by the Radiation Transport Group at Los Alamos National Laboratory, Los Alamos, New Mexico. MCNP can be used for photon, electron, neutron or coupled particle transport. Cross-section data are interpolated for each discrete particle energy. For photons, the code takes account of incoherent and coherent scattering, the possibility of fluorescent emission after photoelectric absorption, absorption in pair production with local emission of annihilation radiation, and Bremsstrahlung. A continuous slowing down model is used for electron transport that includes positrons, K x-rays, and Bremsstrahlung but does not include external or self-induced fields.

The MCNP-4A code treats an arbitrary three-dimensional configuration of materials in geometric cells bounded by first- and second-degree surfaces and fourth-degree elliptical tori. The cells are defined by the intersections, unions, and complements of the regions bounded by the surfaces. Surfaces are defined by supplying coefficients to analytic surface equations.

MCNP provides six standard photon tallies, all of which are normalized to be per starting particle. The three used in these calculations include surface current (F1), surface flux (F2) and track length estimate of energy deposition (F6). Table A2 shows the quantities actually scored in MCNP before final normalization per starting particle.

Tally	Function Quantity	Units
F1:P	W	-
F2:P	$W / (\|\mu\| * A)$	$1/cm^2$
F6:P	$W * T_l * \sigma_T(E) * H(E) * \rho_a / m$	MeV/g

Table A2. The three types of scoring tallies used in the scattered photon correction calculations.

where W = particle weight

$|\mu|$ = absolute value of cosine of angle between surface normal and particle trajectory

A = surface area (cm^2)

T_l = track length (cm) = transit time * velocity

$\sigma_T(E)$ = microscopic total cross section (barns)

H(E) = heating number (MeV / collision)

ρ_a = atom density (atoms / barn-cm)

m = cell mass (g).

The F1 surface tally estimates the number of particles crossing a surface with the following integral:

$$F1 = \int_A \int_\mu \int_t \int_E J(\vec{r}, E, t, \mu)\ dE\ dt\ d\mu\ dA$$

The scalar current is related to the flux as $J(r,E,t,\mu) = |\mu|\,\Phi(r,E,t)\,A$.

The surface flux is a surface estimator but can be thought of as a limiting case of cell flux when the cell becomes infinitely thin.

$$F2 = \lim_{\delta \to \infty} W\,T_1 / V$$

$$= (W\,\delta / \cos\theta) / (A\,\delta) = W / (A\,|\mu|)$$

As the cell thickness δ approaches zero, the volume approaches $A\delta$ and the track length approaches $\delta / |\mu|$, where $\mu = \cos\theta$, the angle between the surface normal and the particle trajectory. This definition of flux also follows from the relation between flux and current. The units of the flux tally are the same as the units of the source.

The F6 cell heating tally comes from the following track length estimator

$$F6 = \frac{\rho_a}{\rho_g} \int_V \int_t \int_E H(E)\ \Phi(\vec{r}, E, t)\ dE\ dt \frac{dV}{V}$$

where ρ_a = atom density (atoms/barn-cm)

ρ_g = gram density (g/cm^3)

H(E) = heating response.

The units of the heating tally are MeV/g. For photons, the heating response is

$$H(E) = \sigma_T(E)\ H_{avg}(E)$$

where the heating number is

$$H_{avg}(E) = \sum_{i=1}^{3} p_i(E) * (E - \overline{E}_{out})$$

i = 1 incoherent (Compton) scattering with form factors

i = 2 pair production ($E_{out} = 2\,m_o c^2$)

i = 3 photoelectric

This tally appears to best represent dose to the medium. All energy transferred to electrons is assumed to be deposited locally.

A.2 PROBLEM SET-UP:

The geometry of the free-air chamber was developed into an input file for the MCNP code using 28 cells formed from 34 surfaces. Three materials were modeled including aluminum for the free-air chamber, brass for the beam defining aperture and air. The source photon spectra were taken from the data in Chapter 3 and binned into energy bins of 1 keV width.

Methods of variance reduction employed in these calculations include:

1) Energy cutoff, where the transport of particles is continued until their energy is out of range of interest and are terminated. Photon energy cut-off was set to 1 keV. It was selected that electrons deposit their energy at the point of their creation.

2) Source direction biasing, where the isotropic source was biased by sampling from a cone of fixed size positioned along the beam axis.

The accuracy of the code was investigated by first transporting monoenergetic photon beams of 10 and 20 keV through oxygen gas and comparing the results of two different scoring options. The photon flux across a surface, F2:P, was calculated as well as photon heating, F6:P, at three scoring planes within the free-air chamber geometry. Assuming that tally F6 is dose, the mass energy-absorption coefficient can be calculated by dividing the F6

$$D = E \bullet \varphi \bullet (\mu_{en}/\rho)$$

tally by the F2 tally and photon energy. The calculated mass-absorption coefficients are compared with the data from Plechaty et al. [5] in Table A3.

Energy (keV)	MCNP-4A [cm^2/g]	Plechaty [cm^2/g]	% Difference
10	5.266	5.272	- 0.1
20	0.5631	0.5633	- 0.0

Table A3. Comparison of calculated mass energy-absorption coefficients with published data for monoenergetic photon beams transported through oxygen.

Monoenergetic photon beams of 6 and 50 keV were each transported through the free-air chamber geometry to see the limits of the photon scatter fraction. The 6 keV beam deposited 0.43% of it's energy in the scatter region, while the 50 keV beam scattered 0.34% of it's energy. The Compton cross section in air is maximum at about 40 keV and varies less than 10% between 15 and 50 keV, the energy range of this study, so only small variations in scatter are expected with changes in the beam photon energy spectra.

Calculations were performed for the free-air chamber geometry as used, plus variations in aperture diameter and material. The scatter fraction was calculated by taking the ratio of energy per unit mass deposited, F6:P tally, in the aperture defined primary beam to that deposited outside the primary beam. This ratio was calculated at three positions along the beam axis inside the free-air chamber volume. The correction factor used in the free-air ionization chamber exposure calculations was the simple average of these three correction factors.

A.3 Results:

The energy deposited per unit mass in the primary region from unscattered photons varied by less than 0.15% when aperture radii were varied from 0.25 to 0.5 cm. This variation is well below the statistical precision of about 1.2% in the primary region. The

energy deposited per unit mass outside the primary region, referred to as scattered region, varied with the square of the aperture radius. This implies that the photon scatter is scatter from the air and not from the aperture itself. Doubling the aperture radius quadrupled the number of photons in the primary beam and increased the photon scatter by nearly a factor of four. To ensure that the scatter source was not the aperture itself, a calculation was performed with an aperture of 0.5 cm diameter and a thickness of 0.15 cm. Both primary and scatter energy deposited per unit mass were statistically the same as for the 0.5 cm diameter, 1.0 cm thick aperture.

The results of the calculations are shown in Tables A4 for the tungsten anode beams and A5 for the molybdenum anode beams. Note that the correction factor varies very little with changes in beam energy or with anode material as the Compton cross section is relatively constant over the energy range of the photon spectra.

The only previous data for photon scatter correction factors are the experimental data from Ritz [1], for tungsten beam energies of 20 to 100 kVp, and Attix and DeLaVergne [2], for beam energies of 60 to 100 kVp. In the region of overlap for these two data sets, the data agree to between 0.2 to 0.3 per cent, strattling the data calculated in this study.

Table A4 Calculated scatter photon correction factors for tungsten anode beams.

Beam code	f_s
20-M	0.0032
30-M	0.0029
40-M	0.0026
50-M	0.0027
30-L	0.0029
40-L	0.0027

Table A5 Calculated scatter photon correction factors for molybdenum anode beams.

Beam code	f_s
Moly25	0.0029
Moly28	0.0029
Moly30	0.0028
Moly35	0.0027
Moly40	0.0026

A.4 REFERENCES:

[1] V. H. Ritz, "Design of Free-Air Ionization Chambers for the Soft X-ray Region (20-100 kv)," Radiology **73** (6):911-922, 1959.

[2] F. H. Attix and L. DeLaVergne, "Plate-Separation Requirements for Standard Free-Air Ionization Chambers," J. Research NBS **53**: 393, 1954.

[3] J. F. Briesmeister, "MCNP - A general Monte Carlo N-Particle transport code, version 4A," Los Alamos National Laboratory Report, LA-12625 (1993).

[4] J. S. Hendricks and J. F. Briesmeister, "Recent MCNP developments," Los Alamos National Laboratory Report, LA-UR-91-3456 (1992).

[5] E. F. Plechaty, D. E. Cullen, and R. J. Howerton, " Tables and Graphs of Photon-Interaction Cross Sections From 0.1 keV to 100 MeV Derived From the LLL Evaluated-Nuclear-Data Library," UCRL-50400, Vol. 6, Rev. 3 (1981).

BIBLIOGRAPHY

AAPM Report No. 29. Equipment requirements and quality control for mammography. Report of Task Group No.7: Diagnostic x-ray imaging, Martin J. Yaffe, chairman. New York: *Am Assoc. Physicists Med*; August 1990.

American College of Radiology, Committee on Quality Assurance in Mammography. Medical Physicist's Manual. American Cancer Society (1992).

F.H. Attix, *Introduction to Radiological Physics and Radiation Dosimetry*, John Wiley and Sons, New York (1986).

F.H. Attix, "Electronic Equilibrium in Free-Air Chambers and a Proposed New Chamber Design," Naval Res. Lab. Rep. No. 5646 (1961).

F.H. Attix and L. DeLaVergne, "Plate-Separation Requirements for Standard Free-Air Ionization Chambers," Journal of Res.of the Nat.Bur. of Standards, **53**, 393-402 (1954).

J.F. Briesmeister, "MCNP - A general Monte Carlo N-Particle transport code, version 4A," Los Alamos National Laboratory Report, LA-12625 (1993).

H-P Chan, Ph.D. dissertation University of Chicago, USA (1981).

C.S. Chen, K. Doi, C. Vyborny, H.P. Chan and G. Holje, "Monte Carlo simulation studies of detectors used in the measurement of diagnostic x-ray spectra," Med. Phys. **7**, 627-635 (1980).

J.G. Coletti, D.W. Pearson, and L.A. DeWerd "Mammography exposure standard: Design and characterization of a free-air ionization chamber," Rev. Sci. Instrum. **66**(3), 2574-2577 (1995).

J.G. Coletti, D.W. Pearson, C.M. Johnson, P.J. Lamperti, and L.A. DeWerd, "Comparison of Exposure Standards in the Mammography X-ray Region," submitted to Medical Physics (1995).

B.J. Conway, O.H. Suleiman, F.G. Rueter, R.G. Antonsen, and R.J. Slayton, "National Survey of Mammographic Facilities in 1985, 1988 and 1992," Radiology 1994; **191**: 323-330.

H-P Chan and K.Doi, "Physical Characteristics of scatter radiation in diagnostic radiology; Monte Carlo simulation studies," Med. Phys. **12**, 152-165 (1985).

T.R. Fewell and R.E. Shuping, "Photon energy distribution of some typical diagnostic x-ray beams," Med. Phys. **4**, 187-197 (1977).

T.R. Fewell and R.E. Shuping, "Handbook of mammographic x-ray spectra," HEW Publication (FDA) 79-8071 (1978).

T.R. Fewell and K. E. Weaver, "The measurement of diagnostic x-ray spectra with a high purity germanium spectrometer," Proc. SPIE **56**, 4 (1975).

J.R. Gentry and L.A. DeWerd, "TLD Measurements of In-Vivo Mammographic Exposures and the Calculated mean glandular dose across the United States," submitted to Med. Phys. (1995).

J.S. Hendricks and J.F. Briesmeister, "Recent MCNP developments," Los Alamos National Laboratory Report, LA-UR-91-3456 (1992).

J. H. Hubble, "Photon mass attenuation and energy-absorption coefficients for 1 keV to 20 MeV," Int. J. Appl. Radiat. Isot. **33**, 1269-1290 (1982).

R.F. Laitano and M.P. Toni, "The primary exposure standard of ENEA for medium energy x-rays. Characteristics and measurement procedures." Report RT/PROT (83) 27,

Laboratorio di Metrologia della Radiazioni Ionizzani ENEA, CRE Casaccia, c.p. 2400 Roma, Italia (1984).

P.J. Lamperti, T.P. Loftus and R. Loevinger, "Calibration of X-Ray and Gamma-Ray Measuring Instruments," NBS Special Publication 250-16 (1988).

J. Law, "Calibration of ion chambers for use in mammography," Br. J. Radiol. **66**: 51-54 (1993).

Mammography Quality Standards Act of 1992, Public Law 102-539.

C.M. Meger, "Dosimetry and Radiobiology of Synchrotron Produced Ultrasoft X-rays," Ph.D. thesis, UW-Madison (1989).

National Research Council, Committee on the Biological Effects of Ionizing Radiation. Health Effects of Exposure to Low Levels of Ionizing Radiation (BEIR V). Washington, D.C.: National Academy Press, (1991).

"The National Strategic Plan for the Early Detection and Control of Breast and Cervical Cancers," U.S. Department of Health and Human Services, 1993.

V.H. Ritz, "Design of Free-Air Chambers for the Soft X-Ray Region (20-100 kV)," Radiology, **73**, 911-922 (1959).

V.H. Ritz, "Standard Free-Air Chamber for the Measurement of Low-energy X-rays (20 to 100 Kilovolts-Constant-Potential)," Journal of Res. of the Nat. Bur. of Standards, 64C, 49-53 (1960).

S.M. Seltzer, "Calculated Response of Intrinsic Germanium Detectors to Narrow Beams of Photons with Energies up to ~300 keV," Nuclear Instruments and Methods 188(1981) p. 133-151.

E. Storm and D.W. Lier, "X-Ray Spectrum Distributions in Roentgens," Health Physics **23**, 73 (1972).

E.D. Trout, J.P. Kelley, and A.C. Lucas, "Determination of Half-Value Layer," Am. J. Roentgenol, **84**, 729-740 (1960).

D. M. Tucker, G. T. Barnes, and X. Wu, "Molybdenum target x-ray spectra: A semiempirical model," Med. Phys. **18**, 402-407 (1991).

L.K. Wagner, B.R. Archer, and F. Cerra, "On the Measurement of Half-value Layer in Film-screen Mammography," Med. Phys. **17**, 989-997 (1990).

L.K. Wagner, D.P. Fontenla, C. Kimme-Smith, L.N. Rothenberg, J. Shepard, and J.M. Boone, "Recommendations on performance characteristics of diagnostic exposure meters: Report of AAPM Diagnostic X-ray Imaging Task Group No. 6," Med. Phys. **19,** 231-241 (1992).

R.C. Weast, ed., *CRC Handbook of Chemistry and Physics*, 66th ed., (CRC Press, Boca Raton, FL, 1985)

X. Wu, G.T. Barnes, and D.M. Tucker, "Spectral dependence of glandular tissue dose in screen-film mammography," Radiology **179**: 143-148 (1991).